Numerical Analysis on Wave Load Reduction Effect of a Solid Wall with Porous Plate by Macroscopic CFD Approach

Dongsheng Qiao[1], Jun Yan[1*], Changlong Feng[1, 2], Haizhi Liang[3], Dezhi Ning[1**], Binbin Li[4], Lars Johanning[5]

1. State Key Laboratory of Coastal and Offshore Engineering, Dalian University of Technology, Dalian 116024, China;
2. CCCC Water Transportation Consultants Co. Ltd. Qingdao Branch, Qingdao 266071, China;
3. School of Civil Engineering, Qingdao University of Technology, Qingdao 266033, China;
4. Shenzhen International Graduate School, Tsinghua University, Shenzhen 518055, China;
5. Renewable Energy Group, CEMPS, University of Exeter, Penryn Campus, Penryn, Cornwall TR10 9FE, UK.

Abstract: The porous structures are widely designed in coastal and ocean engineering to reduce the wave load. A macroscopic CFD approach is established to study the wave interaction with a porous plate placed in front of a solid wall. The established numerical wave tank was firstly validated by the analytical results of a vertical wall, and the macroscopic CFD model was validated by the experimental results of a single vertical porous plate. Then the wave load reduction effect of a solid wall with a vertical porous plate in front is investigated, the influences of porosity and relative gap width are compared, and the effects of wave height are also analyzed. The results demonstrate that the porosity and relative gap width are the main effect factors to the wave force reduction effect, and the wave forces on structure increase almost linearly with the increase of relative wave height, while the wave load reduction coefficient and refection coefficient are not linearly. A porosity of 0.2 and relative gap width of 0.2~0.3 are deemed to be optimal geometry parameters at which the wave load reduction effect is optimal. The total horizontal wave force increases nonlinearly with the increase of wave heights, and the quadratic pressure drop condition is essential when studying the wave force on thin porous structures.

Keywords: Porous plate; offshore structures; wave load; CFD simulation; macroscopic approach.

* Corresponding author. Email address: junyan@dlut.edu.cn;

** Corresponding author. Email address: dzning@dlut.edu.cn.

1. Introduction

The wave loads are usually the dominant loads in the design of ocean engineering structures when suffering from the complex ocean environmental loads. With the rapidly development of ocean engineering construction, the investigations on reducing wave force of ocean engineering structures are of great importance. The porous structures, such as the rubble mound breakwater (Andersen et al., 2011), slotted floating box-type breakwaters (Huang et al., 2014), fixed permeable caisson breakwaters (Yueh and Chuang, 2009), submerged porous breakwaters (Na'im et al., 2018), and wave absorbing chambers of floating offshore base (Kou et al., 2016), have been applied in the coastal and ocean engineering structures to absorb wave impact and protecting structures, and the investigations on the interaction between waves and porous structures are one of the key design issues.

Using wave tank test to investigate the interaction between waves and porous structures have been conducted by many scholars. A large-scale model test was carried out by Bergmann and Oumeraci (1998) in the wave tank, and the wave pressure distribution on the porous walls was investigated. Chen et al. (2002) carried out a series of regular wave experiments on perforated caisson in the wave tank and studied the relationships between the reflection coefficient and the structure sizes, including the relative width of the wave absorbing chamber, the porosity, and the relative wave height. Ajiwibow (2011) conducted a 2-D model test to measure the effectiveness of perforated skirt breakwater for short-period waves and analyzed the relationship between the transmission coefficient and non-dimensional variables (skirt draft/incident wave height). A 3-D tank test was performed by Lee et al. (2014) to study the wave heights distribution in terms of evolution phenomena on partially perforated walls, and it was observed that the perforation could reduce wave heights effectively and the perforated wall with side walls performed better on wave height reduction. Liu and Li (2014) conducted experiments to investigate the wave scattering by two-layer horizontal porous plates. Chyon et al. (2017) investigated the interaction between wave and horizontal slotted submerged breakwater by experiments and the effect of size and porosity of the structure on the reduction of wave height. Fang et al. (2018) proposed a four-layer submerged horizontal porous plate breakwater and also discussed the design of the geometrical parameters by 2-D model tests in the wave tank. Through an experimental study on the interaction between solitary waves and vertical porous plates,

Francis et al. (2020) investigated the porosity effect on the dissipation of wave energy and found that the plate porosity ranging 0.1~0.2 gave the optimal energy dissipation.

The tank tests are usually limited by the experimental conditions, such as the secondary refection effect of wave-maker boundary and the accuracy of wave probes and force sensors, and the scale effects also need to be considered. Some investigations concentrated on developing analytical solutions of the interaction of wave-porous structures. For the fluid motion in the porous media, Sollit and Cross (1972) gave a governing equation utilizing the characteristic function expansion method. Dalrymple et al. (1991) systematically studied the reflection and propagation of oblique waves impacting on the porous structures. Teng et al. (2004) studied the interaction between oblique waves and perforated caisson based on the potential flow theory by using characteristic function expansion method, and the variation laws of reflection coefficient and wave force with the incident angle and hole size were also analyzed. Sankarbabu et al. (2008) theoretically investigated the hydrodynamic performance of a breakwater formed by a row of dual cylindrical caisson with a porous outer cylinder, by using a modified characteristic function expansion method. For multi-layers porous plates, Geng et al. (2018) investigated the wave absorbing efficiency based on the linear potential flow theory, and the effects of thickness, porosity, and layout form of plates on wave absorption were also analyzed. Mackay and Johanning (2020) compared two analytical solutions of the interaction between wave and a vertical porous plate, which are derived by two different methods for taking the depth-average of the pressure drop across the porous barrier and neglect the evanescent modes in the wave field. By comparing with the results of Boundary Element Method (BEM) modeling, the two analytical solutions were confirmed to reliable for predicting the wave force on the plate and the transmission and reflection coefficients. Zheng et al. (2020a, 2020b, 2020c) and Koley et al. (2020) developed a semi-analytical model using the linear potential flow theory to investigate the wave scattering of various kinds of porous elastic plates in different water depth conditions. Smith et al. (2020) studied the water-wave scattering by a semi-infinite submerged thin elastic plate using the Wiener-Hopf technique. Mohapatra and Soares (2020) studied the hydroelastic response of a flexible submerged porous plate using the generalized expansion formula based on Green's function.

When the geometry of the physical problem becomes more complicated, the analytical approaches become increasingly difficult. Thus, using numerical approaches

based on the potential theory are widely applied. Liu et al. (2012) proposed a semi-analytical scaled boundary finite element method (SBFEM) to study the interaction between short-crested wave and a concentric cylindrical structure with double-layered perforated walls, and discussed the effects of wave conditions and geometry parameters of the structure on wave force and water surface elevations. Mackay et al. (2019) established an iterative BEM model to solve the quadratic pressure loss across the porous sheet and validated it by comparing the tank tests. Meanwhile, some investigations on the interaction between waves and porous structures were also conducted by the CFD method. Ren and Ma (2015) used the CFD method to establish a 3-D numerical wave tank (NWT) and simulated the interaction between nonlinear waves and perforated quasi-ellipse caissons. It was observed that with the wave period decreased, the wave force on caissons would be diminished, and a smaller transverse distance among caissons would result in higher wave forces. Chen et al. (2019) used Ansys Fluent to create a 2-D NWT and performed simulations on the interaction between waves and a vertical porous wall placed in solid wall front. The effects of gap width and porosity on wave force and reflection coefficient were analyzed.

The potential theory usually cannot well capture the viscous effect, and the CFD investigations listed above usually need a huge number of mesh cells and take a lot of computing time, with the reason of high-quality grids requirement for the fluid field, especially near the boundaries of porous structures. Alternatively, without explicitly establishing the geometric model of porous structures to simulate the microscopic processes of waves and porous structures interaction, the macroscopic mesh-free approaches which is more concerned on the macroscopic effects of the porous structure on incident waves have been proposed. Liu et al. (1999) developed a numerical model to simulate the wave-porous structures interaction, in which the spatially averaged Navier-Stokes equations were applied to describe the flow in porous media, and the empirical linear and nonlinear frictional forms were used to model the drag forces produced by the solid skeleton. The proposed model was applied to analyze the flow passing through a porous dam and the breaking wave overtopping a caisson breakwater protected by porous armor units. A similar CFD model was proposed by del Jesus (2012) for heterogeneous media where porosity varies along the porous body, with three terms that describe the physical process of water flow interacting with porous structures covered in the momentum equations. By comparing the simulated results with

experiments, the proposed model was verified to be reliable. Based on the work of del Jesus, Higuera et al. (2014) established a CFD model for wave/flow-porous structures interaction using OpenFOAM, by analyzing the pressure loss of flows passing through porous structures and adding the pressure loss term into the momentum equation of the porous media region. The established model was applied to porous dam break and the interaction between waves and rubble breakwater, and the comparison with experiments indicated that the established CFD by this macroscopic approach is reasonable. A 3-D large-eddy-simulation model with macroscopic model equations of porous flow was proposed by Wu et al. (2014), and the interaction between solitary waves and permeable breakwaters was studied. It was demonstrated that the results obtained by microscopic and macroscopic modeling both consistent with experiments in terms of water surface elevations and velocity fields. Molines et al. (2020) established a CFD model for the simulation of wave attacking mound breakwaters with parapets by OpenFOAM, where the porous media was modeled by a macroscopic approach. The established model was validated by experiments and then a series of numerical simulation were conducted by the CFD model for evaluating the effects of nine crown wall geometries with and without parapets. Qiao et al. (2020) established a CFD model with quadratic pressure drop condition for simulating the wave interaction with thin porous plate, and the comparison with experimental results shown that the alternative CFD method is feasible. The CFD models above using macroscopic approaches avoided dealing with the complex physical boundary conditions and thus decreasing the mesh numbers. The accuracy is confirmed to be sufficient for predicting the wave force on porous structures and wave surface elevations.

The porous plate or wall is widely used in offshore structures against wave attack, and the wave force reduction effect of a porous plate on offshore structures needs to be further investigated. Based on the research of wave interaction with only a porous plate by the authors (Qiao et al., 2020), a solid vertical wall with a porous plate in front is further investigated in this paper. A NWT is created by ANSYS Fluent, and a macroscopic approach is applied to establish the numerical model for simulating the interaction between waves and vertical porous plate. The established numerical model is firstly applied to the case of interaction between waves and a vertical porous plate. The numerical results are compared with a microscopic approach and model tests, and excellent agreement is obtained. Then the established CFD model is applied to simulate

the interaction between waves and the structure of a solid vertical wall with a porous plate in front. The wave force on the structure and the reflection coefficient are studied with different porosities of porous plate and relative gap width between the porous plate and solid wall.

This paper is organized as follows. The establishment of the NWT and macroscopic pressure loss model of porous plate is presented in Section 2. Section 3 presents the established model validation, including the mesh convergence validation, a case validation for NWT, and a case validation of a vertical porous plate. The CFD simulations and analysis of wave interaction with SWP are presented in section 4. Finally, the conclusions are presented in Section 5.

2. Numerical model

2.1. Governing equations

The Navier-Stokes equations of general form are used to describe the flow in NWT:

$$\frac{\partial u}{\partial x}+\frac{\partial v}{\partial y}=0 \tag{1}$$

$$\frac{\partial u}{\partial t}+u\frac{\partial u}{\partial x}+v\frac{\partial u}{\partial y}+w\frac{\partial u}{\partial z}=-\frac{1}{\rho}\frac{\partial p}{\partial x}+\nu(\frac{\partial^2 u}{\partial x^2}+\frac{\partial^2 u}{\partial y^2}+\frac{\partial^2 u}{\partial z^2}) \tag{2}$$

$$\frac{\partial v}{\partial t}+u\frac{\partial v}{\partial x}+v\frac{\partial v}{\partial y}+w\frac{\partial v}{\partial z}=-\frac{1}{\rho}\frac{\partial p}{\partial y}+\nu(\frac{\partial^2 v}{\partial x^2}+\frac{\partial^2 v}{\partial y^2}+\frac{\partial^2 v}{\partial z^2}) \tag{3}$$

$$\frac{\partial w}{\partial t}+u\frac{\partial w}{\partial x}+v\frac{\partial w}{\partial y}+w\frac{\partial w}{\partial z}=-\frac{1}{\rho}\frac{\partial p}{\partial z}+\nu(\frac{\partial^2 w}{\partial x^2}+\frac{\partial^2 w}{\partial y^2}+\frac{\partial^2 w}{\partial z^2})-g \tag{4}$$

where, u , v and w are the instantaneous velocity; p represents the instantaneous effective pressure; ν is the molecular viscosity. The free water surface in NWT is captured by the VOF (volume of fluid) method (Hirt and Nichols, 1981), and for each control volume, the volume fraction of air and water phases can be described by following equations:

$$\frac{\partial F_i}{\partial t}+F_i\left(\frac{\partial u}{\partial x}+\frac{\partial v}{\partial y}+\frac{\partial w}{\partial z}\right)=0 \tag{5}$$

$$\sum_{i=1}^{2}F_i=1 \tag{6}$$

where, F_i represents the volume fraction of the ith phase.

2.2. Wave generation and absorption

Figure 1 shows the empty NWT, which can generate expected waves on the left boundary and eliminate waves with the wave absorbing region at the end. In this paper, a finite volume method (FVM)-based CFD software, ANSYS Fluent, is used to establish the NWT. A pushing-board method is applied to generate expected regular linear waves in the left boundary of NWT, and following equations can describe the motion of pushing-board:

$$x_b(t) = \frac{S_0}{2}\sin \omega t \tag{7}$$

$$u_b(t) = \frac{\omega S_0}{2}\cos \omega t \tag{8}$$

where, t is the flow time; $x_b(t)$ and $u_b(t)$ represent the displacement and velocity of pushing-board respectively; ω is the wave frequency; S_0 is the stroke of pushing-board, which is related to the parameters of the expected wave. The surface elevation of wave generated by pushing-board can be expressed as equation (9) (Li and Teng, 2015), from which the relationship between S_0 and the parameters of the expected wave can be obtained as equation (10):

$$\eta(x,t) = \frac{S_0}{2}\frac{4\sinh^2(kd)}{2kd + \sinh(2kd)}\cos(kx - \omega t) = \frac{H}{2}\cos(kx - \omega t) \tag{9}$$

$$S_0 = \frac{2kd + \sinh(2kd)}{4\sinh^2(kd)}H \tag{10}$$

where, η represents the wave surface elevation; k represents the wave number; d represents the water depth; H represents the wave height. The velocity of the pushing-board is controlled as equation (8) by Users Define Function (UDF) of Fluent, and then the wave can be generated as equation (9) expressing.

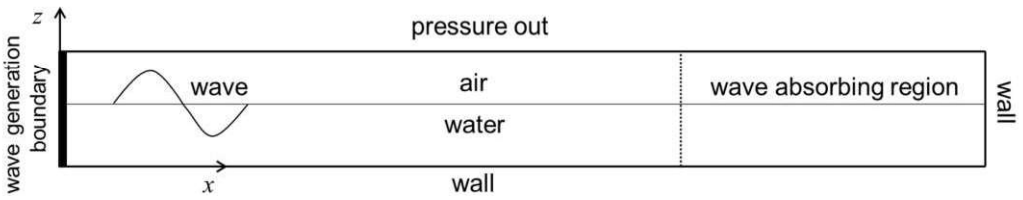

Fig. 1 Numerical wave tank (NWT)

A wave absorbing region is set at the end of the tank to eliminate the reflection wave, where the linearly increasing damping is applied, and the damping source terms are added into the momentum equations. The momentum equations with added

damping source terms can be expressed as (Madsen, 1983):

$$\frac{\partial u}{\partial t}+u\frac{\partial u}{\partial x}+v\frac{\partial u}{\partial y}+w\frac{\partial u}{\partial z}=-\frac{1}{\rho}\frac{\partial p}{\partial x}+\nu(\frac{\partial^2 u}{\partial x^2}+\frac{\partial^2 u}{\partial y^2}+\frac{\partial^2 u}{\partial z^2})-\mu(x)u \tag{11}$$

$$\frac{\partial v}{\partial t}+u\frac{\partial v}{\partial x}+v\frac{\partial v}{\partial y}+w\frac{\partial v}{\partial z}=-\frac{1}{\rho}\frac{\partial p}{\partial y}+\nu(\frac{\partial^2 v}{\partial x^2}+\frac{\partial^2 v}{\partial y^2}+\frac{\partial^2 v}{\partial z^2})-\mu(x)v \tag{12}$$

$$\frac{\partial w}{\partial t}+u\frac{\partial w}{\partial x}+v\frac{\partial w}{\partial y}+w\frac{\partial w}{\partial z}=-\frac{1}{\rho}\frac{\partial p}{\partial z}+\nu(\frac{\partial^2 w}{\partial x^2}+\frac{\partial^2 w}{\partial y^2}+\frac{\partial^2 w}{\partial z^2})-g-\mu(x)w$$

where, the damping coefficient $\mu(x)$ is expressed as:

$$\mu(x)=\begin{cases}0 & ,\ for\ x\le x_1\ or\ x\ge x_2\\ \alpha\dfrac{(x-x_1)}{(x_2-x_1)} & ,\ for\ x_1<x<x_2\end{cases} \tag{13}$$

where, x_1 and x_2 are the start and end of wave absorbing region; α is an empirical coefficient, which is set as 8.0 in this paper.

2.3. Porosity implementation

As stated in Section 1, compared to the microscopic CFD approach, the macroscopic CFD approach not only can avoid huge computational cost but also have sufficient accuracy for simulating wave-porous structures interactions. The macroscopic porosity effect can be represented by an averaged pressure loss through the porous media (Mackay and Johanning, 2020), where the detailed geometry does not need to be resolved explicitly. This subsection will analyze the pressure loss of interaction between waves and vertical porous plate.

Darcy (1856) found that when water flowing through sand, the hydraulic gradient can be assumed to be linearly proportional to the flow passing through, as shown in the flowing equation:

$$I=-\frac{1}{\rho g}\frac{\partial p}{\partial y}=a_p\bar{u} \tag{14}$$

where, I is the hydraulic gradient, a_p is an empirical coefficient. $\bar{u}$ is averaged discharge velocity. In the work of Forcheimer (1901), more energetic flows with high Reynolds number were considered, and Darcy's law was thus extended by adding a quadratic term:

$$I=-\frac{1}{\rho g}\frac{\partial p}{\partial y}=a_p\bar{u}+b_p\bar{u}|\bar{u}| \tag{15}$$

where, b_p is an empirical coefficient. Polubarinova-Kochina (1962) considered the added mass effects of unsteady flows and added the transient term into the formulation:

$$I = -\frac{1}{\rho g}\frac{\partial p}{\partial y} = a_p \bar{u} + b_p \bar{u}|\bar{u}| + c_p \frac{\partial \bar{u}}{\partial t} \tag{16}$$

where, c_p is an empirical coefficient. Sollitt and Cross (1972) further proposed that when a wave passing through a vertical thin porous barrier, the pressure loss ΔP can be expressed as:

$$\frac{\Delta P}{\rho} = \frac{\nu \boldsymbol{U}}{l} + \frac{C_f}{2}\boldsymbol{U}|\boldsymbol{U}| + c\frac{\partial \boldsymbol{U}}{\partial t} \tag{17}$$

where, ν is the molecular viscosity; l is a length scale, which is related to geometry characteristics of porous structures; c is an inertial coefficient; $\boldsymbol{U}$ represents the velocity normal to the plate; C_f is a dimensionless friction coefficient, which can be expressed as (Molin, 2011):

$$C_f = \frac{1-\varepsilon}{\varepsilon^2 \delta} \tag{18}$$

where, ε represents the porosity of porous plate; δ is the discharge coefficient, usually taken as 0.4–0.5 (Mackay and Johanning, 2020), and it is chosen as 0.5 in this paper. The first term in the right of equation (16) is a linear viscous friction term, the second term is a quadratic turbulent dissipation term, and the third term is a inertia term. The linear viscous friction term is dominant at low Reynolds number while the quadratic turbulent dissipation term becomes dominant at high Reynolds number (Sollitt and Cross, 1972). The Reynolds numbers for wave interaction with thin porous plates are usually sufficiently high so that the linear viscous friction term can be neglected (Mackay and Johanning, 2020). The inertia term accounts for added mass effects and transient interaction between the fluid and porous structures. The inertial coefficient c is related to the geometries of porous structures. For a porous plate with circle holes, the inertial coefficient c can be calculated by the following equation (McIver, 1998):

$$\frac{c}{s} \approx 0.3898\varepsilon - 0.03239\sqrt{\varepsilon} + 1.2415 + \frac{0.8862}{\sqrt{\varepsilon}} \tag{19}$$

where, s represents the distance between adjacent hole centers.

To model wave flow passing through the porous plate, the pressure loss per unit

thickness is added into the horizontal momentum equation in the geometric region of porous plate as a source term. According to equations (17) and (18), the added source term S_{porous} can be expressed as:

$$S_{porous} = -\frac{1}{\rho}\frac{\Delta P}{\Delta n} = -\frac{1}{\Delta n}\left(\frac{1-\varepsilon}{2\varepsilon^2\delta}u|u| + c\frac{\partial u}{\partial t}\right) \tag{20}$$

where, Δn is the thickness of porous plate.

3. Numerical model validation

3.1. Mesh convergence validation

Figure 2 shows the generated mesh of an empty NWT. In *x*-direction, the mesh size is defined to 1/10 of S_0 in the moving region of pushing-board, Δx in the wave propagation region, and changes to sparse gradually in the wave absorbing region. In y-direction, the mesh size is defined to Δy in the one wave height region, and changes to sparse gradually in the remaining region.

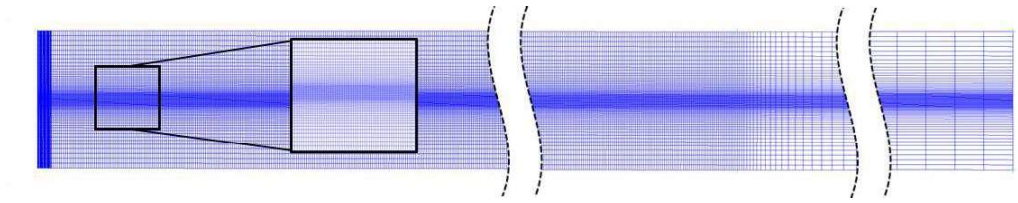

Fig. 2 Mesh refinement

For mesh convergence validation, four mesh types are considered as Table 1 shown. The same wave condition (T=1.9s, H=0.0772m, d=1.0m, L=4.85m) is generated in the NWT under different mesh characteristics. After comparing the wave surface elevations under four different mesh types with the theoretical solution, the mesh type 2 where $\Delta y = 1/10H$, $\Delta x = 1/160L$ is selected due to its enough high simulation precision and a relatively smaller number of mesh cells.

Tab. 1 Results of simulated wave height under different mesh types

Mesh type	mesh1	mesh2	mesh3	mesh4
H/Δy	5	10	15	20
λ/Δx	80	160	240	320
Δy(m)	0.0154	0.0077	0.0051	0.0039
Δy (m)	0.0606	0.0303	0.0202	0.0152
wave height (m)	0.0763	0.0768	0.0768	0.0769
relative tolerance	-1.15%	-0.52%	-0.43%	-0.39%

3.2. Model Validation: a vertical wall

A solid vertical wall occupying the full water column is conducted to validate the established NWT. As shown in Figure 3, the solid wall with 1.5m height is set at 25m from the wave-making board. The mesh refinement is shown in Figure 4, which is the same as the empty NWT in Figure 2, except for the mesh cells nearby the solid wall which are further defined as 1/10 of the wall thickness. A regular wave with H =0.0772m, T =1.9s, d =1.0m is generated in the NWT.

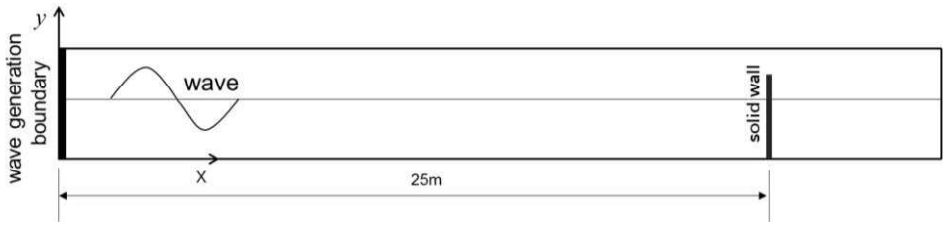

Fig. 3 The layout of NWT with vertical solid wall

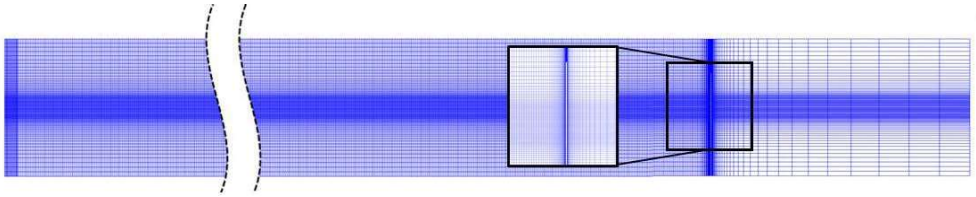

Fig. 4 Generated mesh of NWT with a solid vertical wall

It is known that a standing wave occurs when a regular wave reflected by a vertical wall. Figure 5 shows the time series of water surface elevation at the vertical solid wall. It can be obtained that the average wave height is 1.538m, only 0.38% differing from the analytical value, which is equal to two times of the incident wave height. Figure 6 shows the time series of horizontal wave force on the vertical solid wall, and it can be obtained that the average maximum wave force is 508.82N. The analytical solution of the wave force on the vertical solid wall can be obtained by integrated the pressure on the wall along with the water depth, which can be calculated by following equations (Li and Teng, 2015):

$$p(z) = \rho g H \frac{\cosh k(z+d)}{\cosh kd} \tag{21}$$

$$f = \int_d^\eta p(z)dz = \int_d^0 \rho g H \frac{\cosh k(z+d)}{\cosh kd} dz + O(\varepsilon^2) \approx \frac{\rho g H}{k} \tanh kd \tag{22}$$

where, $p(z)$ is the relative pressure on the solid wall along with the depth; f is horizontal wave force on the wall. It can be obtained that the analytical wave force on the wall is 502.11N, and the numerical wave force is only 1.34% differing from the

analytical values. The results above have validated that the established NWT is reliable.

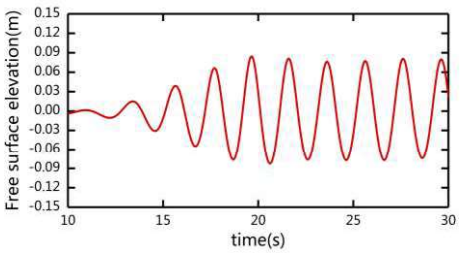

Fig. 5 Time series of free surface elevation at x=25m

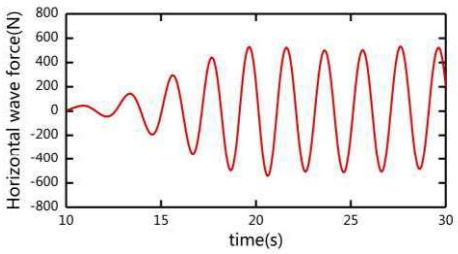

Fig. 6 Time series of horizontal wave force on the solid wall

3.3. Model Validation: a single porous plate

The established CFD model using the macroscopic approach is firstly applied to the wave interaction with a vertical porous plate for validation. The presented model is respectively compared with a microscopic approach and model tests.

3.3.1. Comparison with a microscopic approach

Figure 7 shows the layout of the NWT with a porous plate under the presented macroscopic CFD model. Figure 8 shows the generated mesh, which is the same as the empty NWT in Figure 2 except for the mesh of porous layer being refined as 1/10 of the porous thickness and the nearby mesh being refined correspondingly. The used porous plate in this subsection is 1.5m in height, 1.0m in width, and 1cm in thickness, and the porosity is 0.3. The corresponding CFD simulation under the microscopic approach is conducted with a 3-D model, and the layout of NWT is the same as Figure 7. Figure 9 simply shows the porous plate used in the microscopic approach, where the interval of circular holes s=25mm and radius r=7.73mm, thus the porosity also being 0.3. The generated mesh of NWT is also the same as Figure 8, except for the mesh nearby the porous plate being refined as Figure 10 shown. A regular wave condition of H=0.0772m, T=1.9s, d=1.0m is generated in the NWT, and the wave force on the porous plate is monitored.

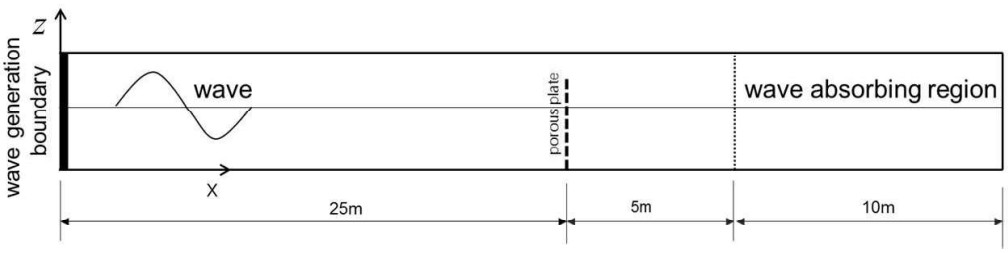

Fig. 7 Layout of NWT with a vertical porous plate

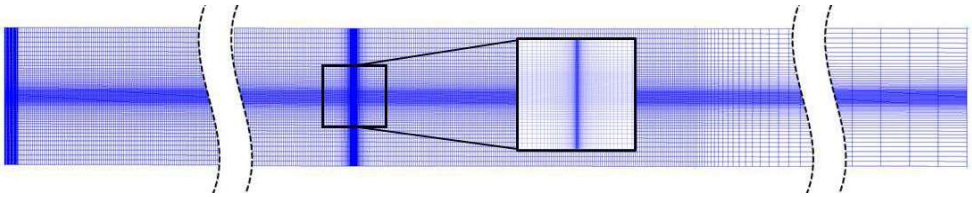

Fig. 8 Generated mesh of NWT with a porous plate under presented CFD model

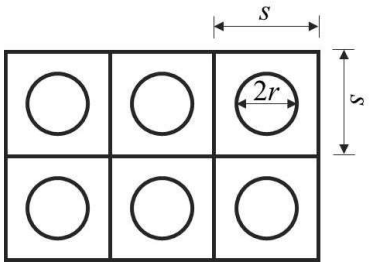

Fig. 9 Illustration of a regular grid of holes in porous plates

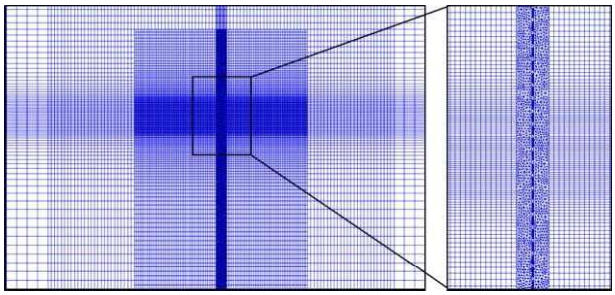

Fig. 10 Generated mesh nearby the porous plate under microscopic approach

Figure 11 shows the comparison of the monitored horizontal wave force between the two approaches. It can be seen that the wave force on the porous plate calculated by the presented macroscopic CFD model is a little larger than the microscopic approach. However, the difference is very small, indicating that the presented macroscopic CFD approach can well substitute the complex microscopic CFD methods in the simulation of wave interaction with a porous plate.

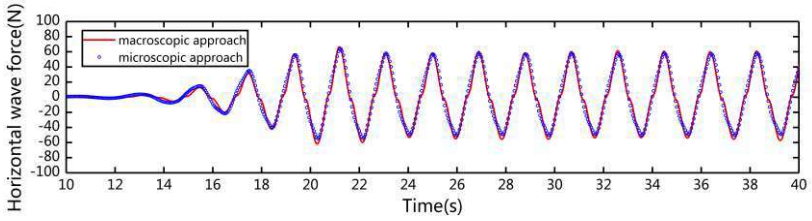

Fig. 11 Time series of horizontal wave force on the porous plate under two CFD approaches

3.3.2. Comparison with model tests

The model tests were conducted at the nonlinear wave flume at Dalian University of Technology (DUT), and the layout in the flume is shown in Figure 12. Two load cells are connected together at the top and bottom sides of the frame to measure the horizontal wave force. A temporarily raised floor was built to install the bottom load cell which is located in a small pit beneath the raised floor. There are five wave probes in total for

monitoring the wave surface elevations. A series of wave conditions with H ranging 0.30~0.772m and T ranging 1.1~1.9s and d=1.0m are applied, and the used porous plate is 1.5m in height, 1m in width, 3mm in thickness and the porosity is 0.2, which also can be simply illustrated as Figure 9. The corresponding CFD simulations using the presented macroscopic model are conducted under the same wave conditions and porous plate parameters, and the layout of NWT is the same as Figure 7, including the same layout of wave probes as model tests.

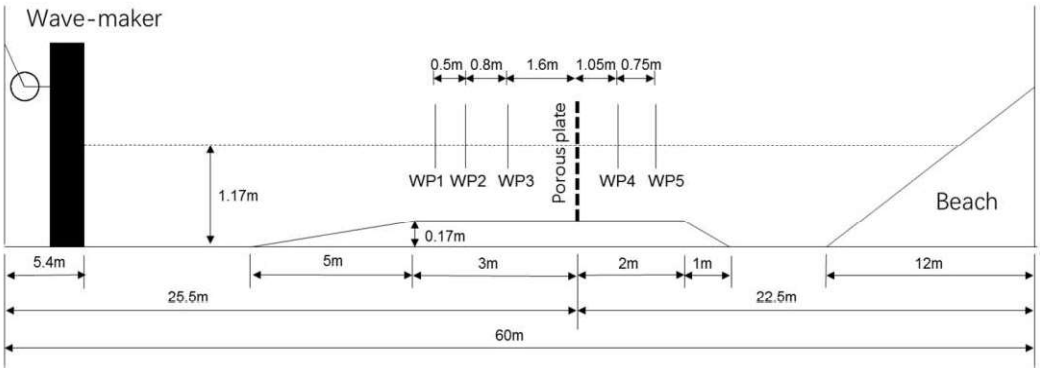

Fig.12 Schematic of the experimental setup in DUT wave flume

Figures 13-14 show the time series of horizontal wave force on the porous plate and the wave surface elevations monitored by wave probes, respectively. Because the distance between wave generated boundary and porous plate are different for CFD simulations and model tests, there is a phase difference between the time series results of two approaches, and the results of model tests are adjusted in phase position for the convenience of comparison. According to Figures 13-14, it can be seen that the CFD results are in good agreement with experiments both in amplitude and phase of horizontal wave force, and the wave surface elevations also show good consistency. The comparing results indicate that the established CFD model is reliable for simulating the interaction between waves and a vertical porous plate.

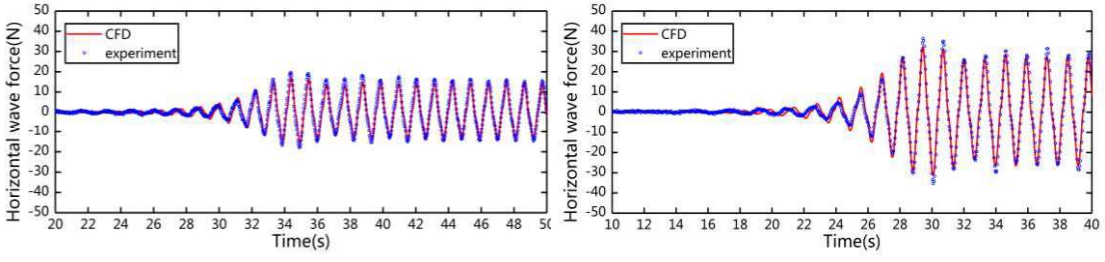

(a) H=0.030m, T=1.1s (b) H=0.0413m, T=1.3s

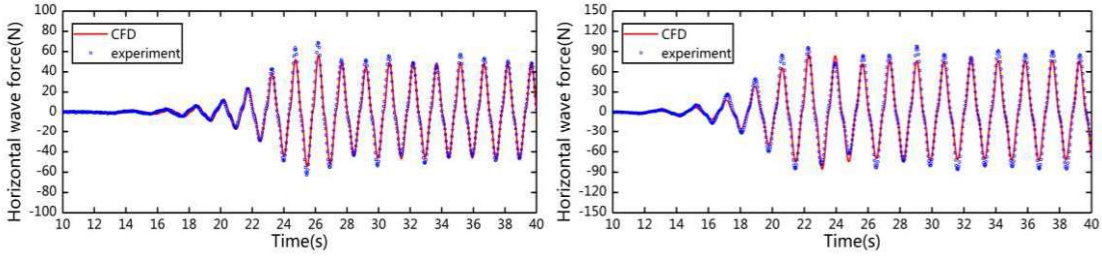

(c) H=0.0533m, T=1.5s (d) H=0.0653m, T=1.7s

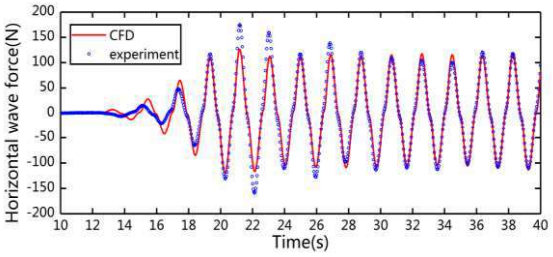

(e) H=0.0772m, T=1.9s

Fig. 13 Time series of horizontal wave force on the porous plate

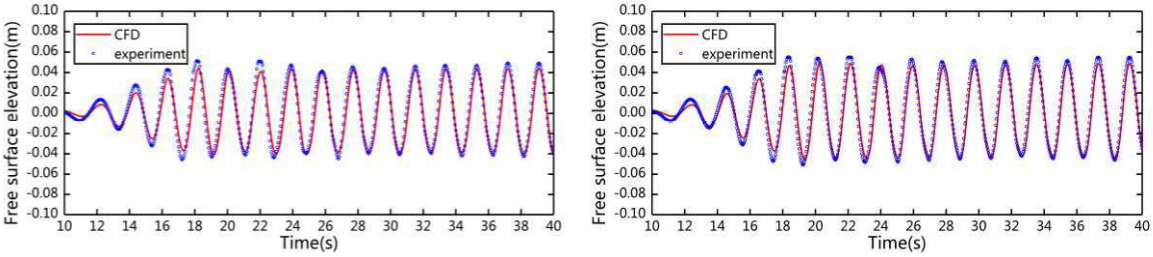

(a) WP1 (b) WP2

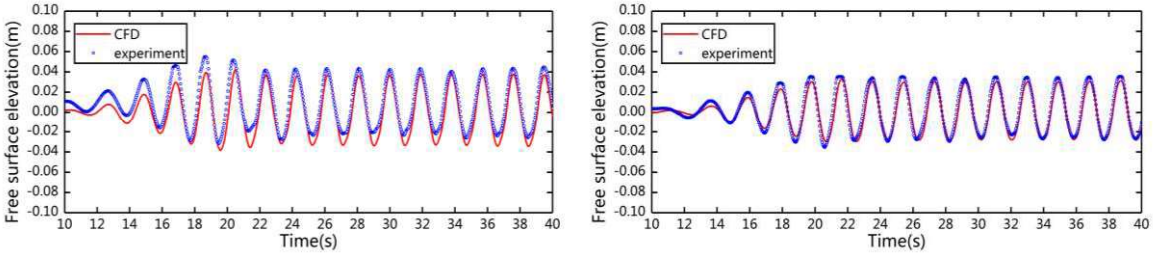

(c) WP3 (d) WP4

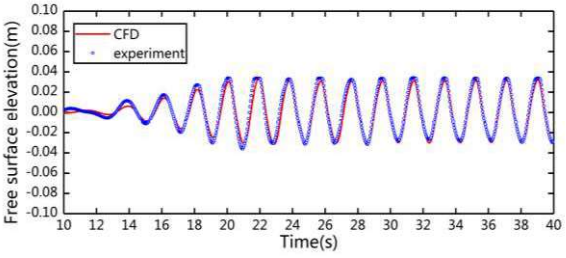

(e) WP5

Fig. 14 Time series of free surface elevations monitored by five wave probes (H=0.0772m, T=1.9s)

4. Simulations results and analysis

The established CFD model is applied to simulate the interaction between waves and the structure of a solid vertical wall with a porous plate in front. The porous plate and solid wall are both 1.5m in height and 1cm in thickness. Figure 15 shows the layout of the NWT with the structure. There are three wave probes set in front of the porous plate for monitoring the reflection waves, and are set as 0.8m, 0.5m, 1.3m apart from each other. The wave forces on the porous plate and solid wall are monitored respectively, and thus the wave force on the whole structure being obtained. Figure 16 shows the generated mesh of NWT including the structure. The wave conditions and model geometry parameters used in this section are shown in Table 2.

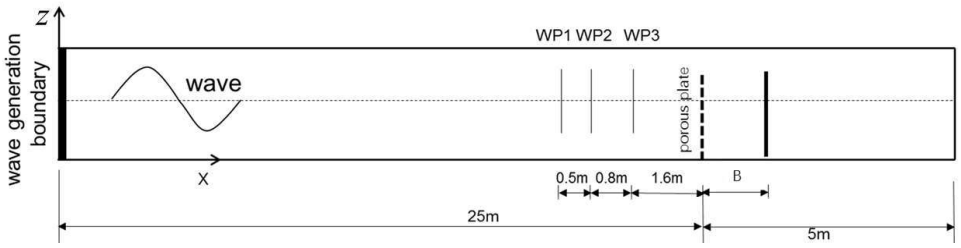

Fig. 15 Layout of NWT including a vertical wall with a porous plate in front

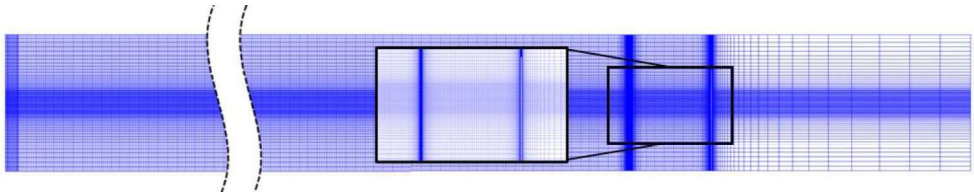

Fig. 16 The generated mesh of NWT including a solid wall with a porous plate in front

Tab. 2 Wave conditions and model geometry parameters

Wave height H (m)	0.16, 0.12, 0.08, 0.04
Wave period T (s)	1.3, 1.5, 1.9, 2.5
Water depth d (m)	1.0
Porosity ε	0.1, 0.2, 0.3, 0.4
Gap width B (m)	0.6, 0.8, 1.0, 1.2

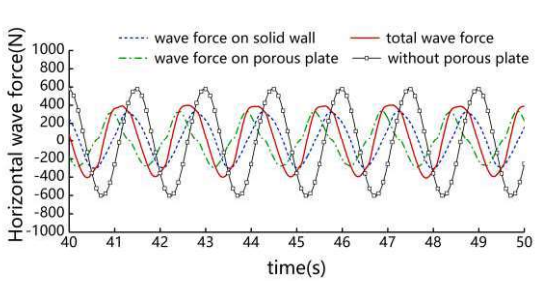

(a) H=0.12m, T=1.5s

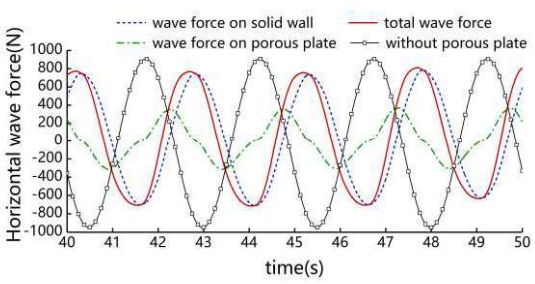

(b) H=0.12m, T=2.5s

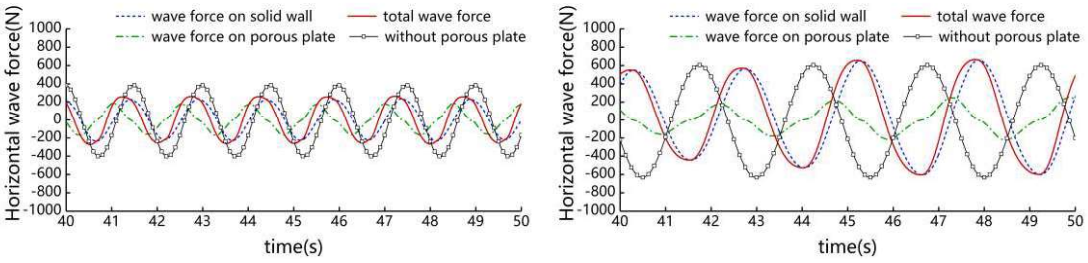

(c) H=0.08m, T=1.5s (d) H=0.08m, T=2.5s

Fig. 17 Time series of horizontal wave force (ε=0.2, B=0.6m)

Figure 17 shows the time series of horizontal wave force on the structure under partial wave conditions with ε=0.2 and B=0.6m. It can be seen that the total wave force on the structure obviously decreases, comparing with the solid wall without a porous plate. It is believed that the decrease is mainly caused by two aspects. Firstly, the porous plate has the impact of dissipating on incident waves, which is mainly related to the porosity. Secondly, there is a phase difference between the wave force on the porous plate and solid wall, which means that partial wave force on the porous plate and solid wall cancels each other out. The phase difference above is mainly related to the gap width B between the porous plate and solid wall, and the wave length L of the incident wave. Therefore, the effects of porosity ε and relative gap width B/L will be analyzed next. For further analysis, the wave force reduction coefficient is introduced to evaluate the wave load reduction effect of the porous plate on the structure, which is defined as the following equation:

$$E_f = \frac{F_{wp} - F_{w0}}{F_{w0}} \tag{23}$$

where, F_{wp} is the wave force on the whole structure with a porous plate and F_{w0} is the wave force on the solid wall without a porous plate. The reflection waves are analyzed at the same time, and the reflection coefficient is defined as:

$$K_r = \frac{H_r}{H_i} \tag{24}$$

where, H_r and H_i are wave heights of reflection and incident wave, respectively. To obtain the reflection wave height, the refection wave and incident wave need to be separated from the wave monitored by wave probes, and the two-point method proposed by Goda and Suzuki (1976) is used.

4.1. Effects of porosity

When an incident wave impacts on the porous plate, some of the wave will be reflected, some will be dissipated, and the remained components will transmit through the porous plate and impact on the solid wall behind. If the porosity is zero, meaning that the porous plate becomes a solid wall, the total wave force will be equal to the wave impacting on a solid vertical wall; in another extreme, if the porosity tends to infinity, meaning that the porous plate does not exist, all components of the incident wave will impact on the solid wall. The maximum total wave force under two extremes above will all approach the largest value. Therefore, an optimal porosity of the porous plate can be expected at which the maximum total wave force being reduced to the smallest value.

Figure 18 shows the time series of total wave force on the structure with different porosities, where the gap width B is fixed as 0.6m. It can be obtained that the amplitude of wave force varies with the porosity of porous plate, meaning that the variation of porosity has a significant effect on the wave force reduction. The effects of porosity on wave force the porous plate and solid wall are shown in Figure 19. It can be obtained that with the increase of porosity, the wave force on porous plate decreases while the wave force on solid wall increases. That is because, with the increase of porosity, the interaction area between wave and porous plate decreases, thus causing the reduction of wave force on it. Meanwhile, more components of incident wave transmit through the porous plate and impact on the solid wall, causing the wave force on it increasing. It also can be inferred from Figure 19 that when the porosity tending to infinity, which means that there is no porous plate and all of the incident wave will impact on the solid wall, the wave force on the porous plate will tend to 0 and the wave force on the solid wall will tend to a constant value, which is approximately equal to the theoretical wave force calculated by equation (23).

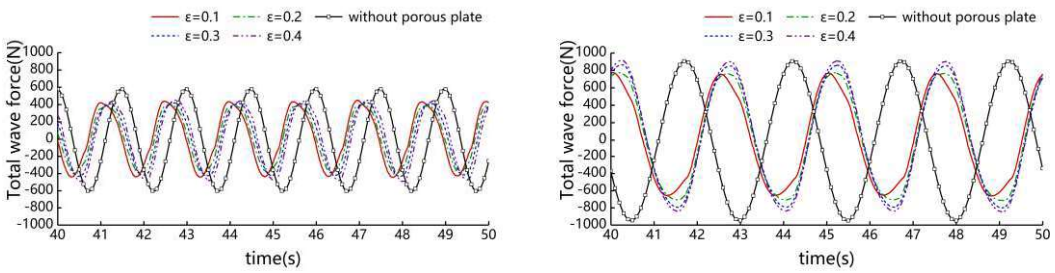

(a) H=0.12m, T=1.5s (b) H=0.12m, T=2.5s

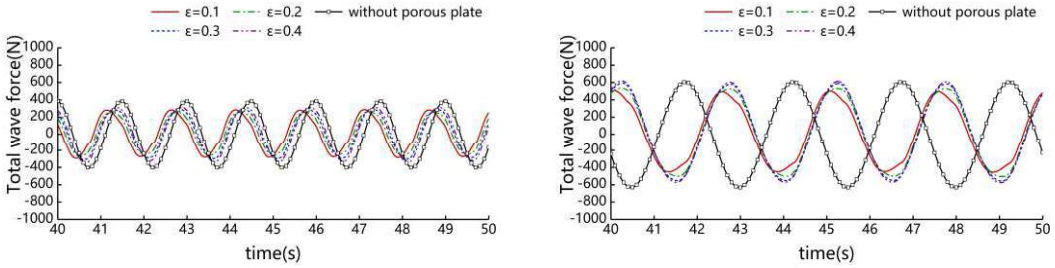

(c) H=0.08m, T=1.5s (d) H=0.08m, T=2.5s

Fig. 18 Time series of total wave force on the structure with different porosities

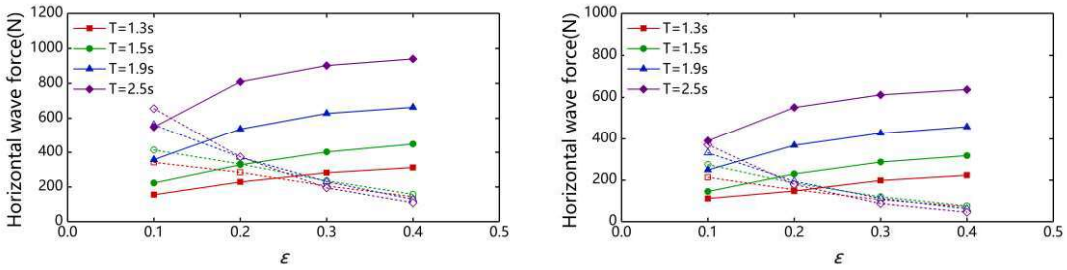

(a) H=0.12m, B=0.6m (b) H=0.08m, B=0.6m

Fig. 19 Maximum wave force on the porous plate and solid wall against ε (dotted lines and hollow marks for the porous plate, solid lines, and marks for the solid wall)

Figures 20-21 show the effect of porosity on E_f and K_r. It is known that, when K_r=1, full-refection occurs and the wave force is the largest; when $K_r<1$, partial refection occurs, and the smaller K_r will also result in the smaller wave force and the larger E_f. In other words, E_f and K_r are negatively correlated, and it can be seen that the variation laws of E_f and K_r in Figures 20-21 are consistent with the law above. It can be learned from Figure 20 that the variation laws of E_f and porosity under different wave conditions are inconsistent. For most wave conditions, E_f reaches the largest value at ε=0.2, except for the wave conditions of H=0.12m, T=1.3s and H=0.08m, T=1.3s, where E_f reaches the largest value at ε=0.1 and 0.3, respectively.

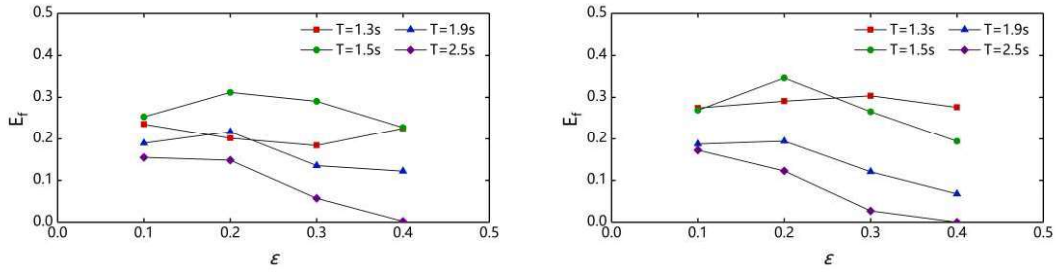

(a) H=0.12m, B=0.6m (b) H=0.08m, B=0.6m

Fig. 20 Effect of porosity on the wave force reduction coefficient

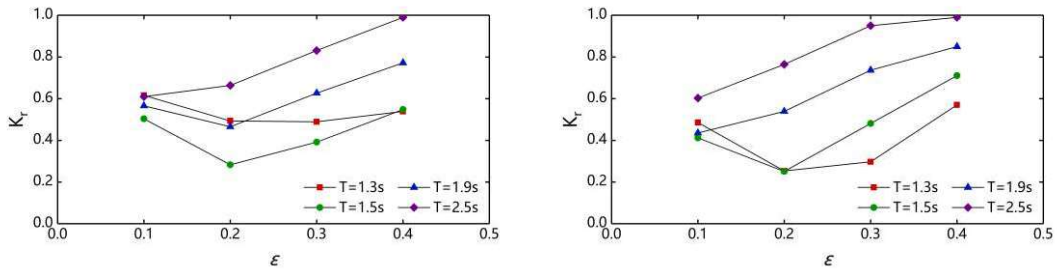

(a) H=0.12m, B=0.6m (b) H=0.08m, B=0.6m

Fig. 21 Effect of porosity on the reflection coefficient

4.2. Effects of relative gap width

The maximum total wave force on the structure is not equal to the sum of maximum wave force on the porous plate and on the solid wall, with the reason of the phase difference between the wave force on them. The phase difference above is related to the gap width B and wave length L. If the porous plate is assumed to have no disturbance on the incident wave, the total wave force on the structure will approach the smallest value when $B/L=0.5$ (or odd times of 0.5). In this case, when the porous plate is impacted by a wave peak, the solid wall is impacted by a wave trough, thus the wave force on the porous plate and solid wall canceling each other out partially, and vice versa. In fact, due to the disturbance of porous plate to the incident wave, the value of B/L at which the total wave force on the structure being the smallest changes. Therefore, an optimal value of B/L ranging 0~0.5 can be expected, at which the total wave force is the smallest under the same conditions. In this subsection, the gap width B is set as 0.6m, 0.8m, 1.0m, 1.2 m, and the corresponding B/L under different wave lengths varies from 0.09 to 0.46. The wave forces on the porous plate, the solid wall, and the whole structure, and the reflection waves under different wave conditions are investigated.

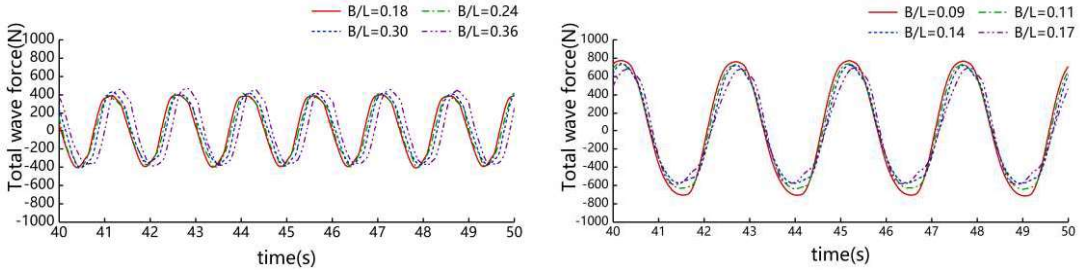

(a) H=0.12m, T=1.5s, ε=0.2 (b) H=0.12m, T=2.5s, ε=0.2

(c) H=0.08m, T=1.5s, ε=0.2 (d) H=0.08m, T=2.5s, ε=0.2

Fig. 22 Time series of total wave force with different B/L

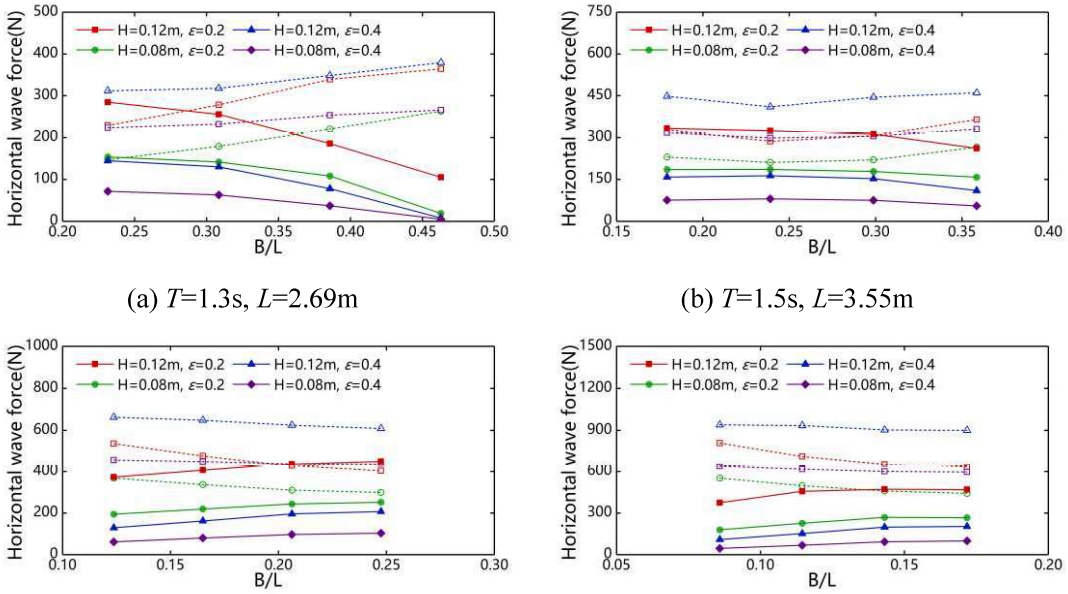

(a) T=1.3s, L=2.69m (b) T=1.5s, L=3.55m

(c) T=1.9s, L=4.85m (d) T=2.5s, L=6.99m

Fig. 23 Maximum horizontal wave force on the porous plate and solid wall against B/L (dotted lines and hollow marks for the porous plate, solid lines and marks for the solid wall)

Figure 22 shows the total wave force on the structure with different relative gap width B/L, and the variation of B/L can cause a reduction of different degrees on total wave force. Figure 23 shows the maximum horizontal wave force on the porous plate and solid wall against B/L. It can be seen that for L=2,69m and 3.55m, where B/L is ranging 0.23~0.46 and 0.18~0.36 respectively, with B/L increases, the wave force on porous plate increases gradually and the wave force on solid wall is opposite;

for $_L$=4.85m and 6.99m, where B/L is ranging 0.12~0.25 and 0.09~0.17 respectively, with B/L increases, the wave force on porous plate decreases gradually and the wave force on solid wall is opposite.

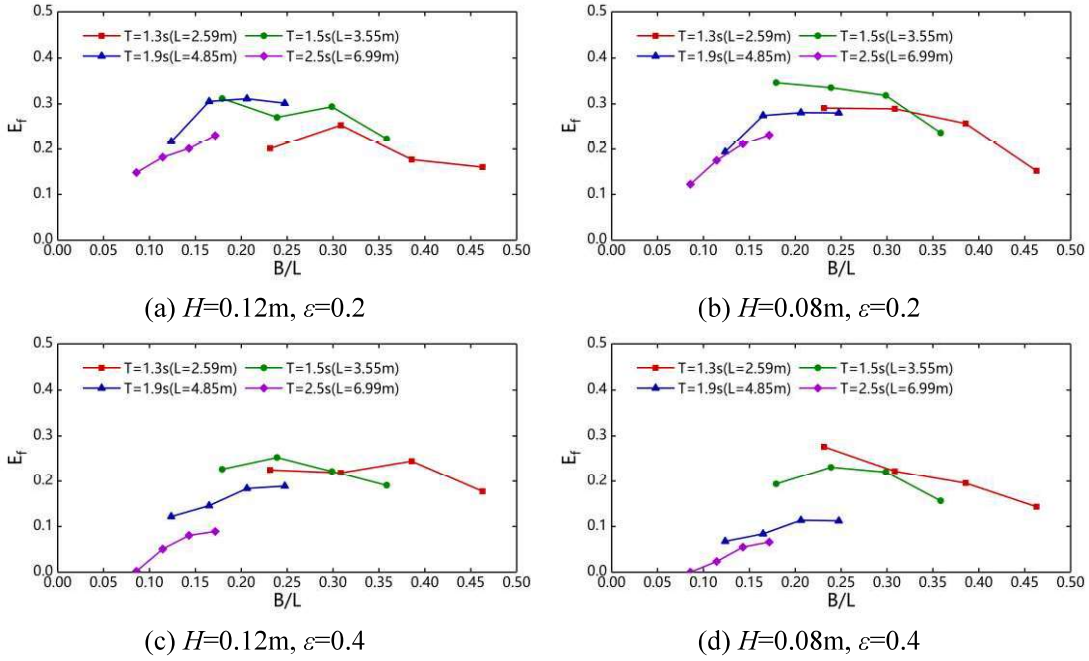

(a) H=0.12m, ε=0.2 (b) H=0.08m, ε=0.2

(c) H=0.12m, ε=0.4 (d) H=0.08m, ε=0.4

Fig. 24 Effect of B/L on wave force reduction coefficient

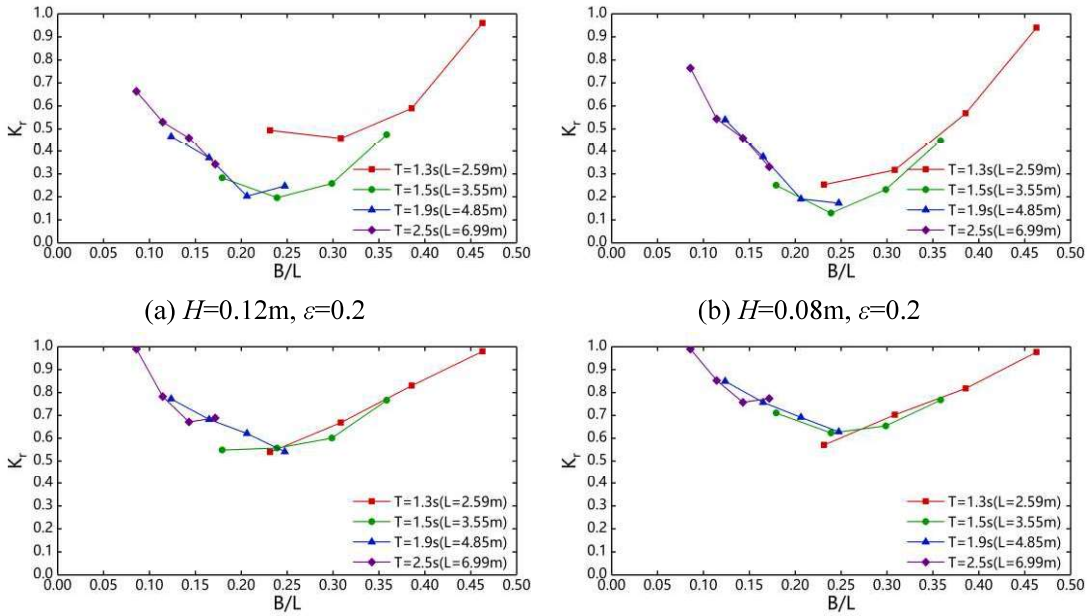

(a) H=0.12m, ε=0.2 (b) H=0.08m, ε=0.2

(c) H=0.12m, ε=0.4 (d) H=0.08m, ε=0.4

Fig. 25 Effect of B/L on the reflection coefficient

Figures 24-25 show the wave force reduction coefficient E_f and reflection coefficient K_r varying against B/L, respectively. It can be seen from the results of

E_f and K_r that some difference occurs when the B/L and other conditions are the same but L is different, which meaning that the wave force reduction effect is different for different wave conditions. On the whole, with B/L increasing from 0 to 0.5, the value of E_f goes up first and then goes down, and the variation of K_r is on the opposite. The largest E_f and smallest K_r appear when B/L ranging from 0.2 to 0.3, where the total wave force is reduced to the smallest.

4.3. Effects of wave height

According to the potential flow theory, the horizontal wave force on a single solid wall increases linearly with the increase of wave heights (Li and Teng, 2015). However, considering the effects of boundary condition of porous barrier for thin porous structures, the relationship between the incident wave height and the wave force on the structures still needed to be studied. In this section, a series of CFD simulations are conducted under different wave heights with the gap width B=0.6m and porosity ε =0.2. The results of present CFD method are compared with a linear potential flow model (Geng et al., 2018).

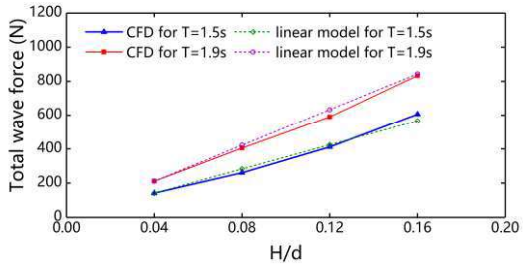

Fig. 26 Wave force varying against H/d by present CFD method and the linear model

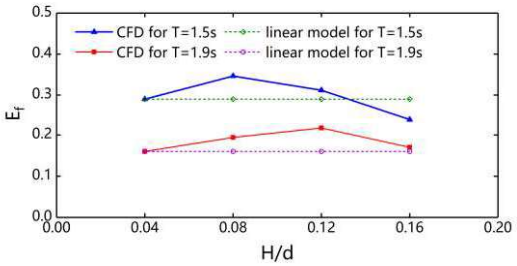

Fig. 27 E_f varying against H/d by present CFD method and the linear model

Figure 26 shows the horizontal wave force amplitude varying against the relative wave heights H/d. It can be seen form Figure 26 that the wave force predicted by the linear model increases linearly with H/d increasing. In contrast, although the wave force predicted by present CFD model also increases with H/d increasing, the relationship between the two is not linear. This will be obvious when comparing the dimensionless coefficient E_f, as shown in Figure 27. The difference above can be explained as follows: according to the Airy wave theory, the motion velocity of water particles in wave is linearly related to wave amplitude, while the wave force on the vertical porous plate is linearly related to pressure drop. This means that the relationship

of velocity and pressure drop determines the relationship of wave force and wave height. Therefore, the linear pressure drop model leads to a linear relationship between the wave height and horizontal wave force on the porous plate and the solid wall, thus the total horizontal wave force is linearly related to the incident wave height. While the present CFD method adopts the quadratic pressure drop condition, and the increase of incident wave amplitude will cause the nonlinear increase of wave force on the porous plate, thus the total horizontal wave force is nonlinear related to the incident wave height. The discussion above illustrated that the quadratic pressure drop condition is essential when studying the wave force on thin porous structures under varying wave heights.

5. Conclusions

For the investigation of the wave load reduction effect of a porous plate on offshore structures, this paper established a CFD numerical model that applied a macroscopic approach for modeling the porous plate. The established CFD model is firstly applied to simulate the interaction between wave and a single vertical porous plate and compared to a microscopic approach and experiment for validation. As a simplified porous structure, a solid wall with a porous plate in front is applied to investigate the wave force reduction effect of the porous plate on the offshore structure. The wave force, wave force reduction coefficient and reflection coefficient were analyzed, with the variation of porosity and relative gap width between the porous plate and solid wall. Several conclusions are obtained as follows:

(1) By comparing with a microscopic CFD approach, it is validated that neglecting the linear and transient terms in pressure loss is reasonable for the CFD numerical model using a macroscopic approach. By comparing with experiments, the established CFD model is validated to be reliable for simulating the interaction between wave and porous plate.

(2) The variation of porosity has effects on wave force reduction. As porosity ε increasing from 0.1 to 0.4, the wave force on the porous plate decreases gradually while the wave force on the solid wall is opposite. The variation of wave force reduction coefficient and reflection coefficient are negatively correlated as expected. The wave force reduction coefficient of whole structure approaches largest at ε=0.2 under most simulated wave conditions except for the wave conditions of H=0.12m, T=1.3s and

H =0.08m, T =1.3s, where E_f reaches the largest value at ε =0.1 and 0.3, respectively.

(3) The gap width between the porous plate and wave length of incident wave influences the phase difference of the wave force on the porous plate and the solid wall, thus affecting the wave force reduction effect. For L=2.69m and 3.55m, as the relative gap width B/L increasing at corresponding ranges, the wave force on porous plate increases gradually, and the wave force on solid wall is opposite; while for L=4.85m and 6.99m, the variation laws above are on the opposite. With B/L increases, the wave force reduction coefficient goes up first and then goes down, and the variation of K_r is on the opposite. The largest E_f and smallest K_r appear when B/L ranging from 0.2 to 0.3, where the total wave force is reduced to the smallest.

(4) The wave height has directly influence on the magnitudes of wave force on the porous structure. The wave force increases nonlinearly with the increase of wave heights, and the quadratic pressure drop condition is essential when studying the wave force on thin porous structures.

Acknowledgments

This work was supported by National Key R&D Program of China [Grant No. 2018YFB1501905], National Natural Science Foundation of China [Grant Nos. 51979030, 51761135011], EPSRC (UK) grant for the project ‘Resilient Integrated-Coupled FOW platform design methodology (ResIn)” [Grant No. EP/R007519/1], and Fundamental Research Funds for the Central Universities.

References

Ajiwibowo H., 2011. 2-D physical modeling to measure the effectiveness of perforated skirt breakwater for short-period waves. ITB Journal of Engineering Science, 43, 57-78.

Andersen T. L., Burcharth H. F., Gironella X., 2011. Comparison of new large and small scale overtopping tests for rubble mound breakwaters. Coastal Engineering, 58(4), 351-373.

Bergmann H., Oumeraci H., 1998. Wave pressure distribution on permeable vertical walls. Coastal Engineering, 2042-2055.

Chen B., Wang L., Ning D., Johanning L., 2019. CFD Analysis on wave load mitigation

effect of a perforated wall on offshore structure. Proceedings of the Twenty-ninth International Ocean and Polar Engineering Conference, Honolulu, Hawaii, USA, 3653-3658.

Chen X. Li Y. Sun D., 2002. Regular waves acting on double-layered perforated caissons. Proceedings of the International Offshore and Polar Engineering Conference, 12, 736-743.

Dalrymple R. A., Losada M. A., Martin P. A., 1991. Reflection and transmission from porous structures under oblique wave attack. Journal of Fluid Mechanics, 224, 625-644.

Darcy H., 1956. Les fontaines publiques de la ville de Dijon. Dalmont, Paris.

del Jesus M., Lara J. L., Losada I. J., 2012. Three-dimensional interaction of waves and porous structures. Part I: Numerical model formulation. Coastal Engineering, 64, 57-72.

Fang Z., Xiao L., Kou Y., Li J., 2018. Experimental study of the wave-dissipating performance of a four-layer horizontal porous-plate breakwater. Ocean Engineering, 151, 222-233.

Forcheimer P., 1901. Wasserbewegung durch Boden. Z. Ver. Dtsch. Ing, 45, 1782-1788.

Francis V., Ramakrishnan B., Rudman M., 2020. Experimental investigation on solitary wave interaction with vertical porous barriers. Journal of Offshore Mechanics and Arctic Engineering-transactions of the ASME, 142(4), 041205.

Geng B., Wang R., Ning D., 2018. The wave absorption efficiency of multi-layer vertical perforated thin plates. Journal of Hydrodynamics, 30(5), 898-907.

Goda, Y., Suzuki Y., 1976. Estimation of incident and reflected waves in random wave experiments. Proceedings of the 15th Coastal Engineering Conference, Honolulu, Hi, ASCE, 828-845.

Higuera P., Lara J. L., Losada I. J., 2014. Three-dimensional interaction of waves and porous coastal structures using OpenFOAM®. Part I: Formulation and validation. Coastal Engineering, 83, 243-258.

Hirt C. W. and Nichols B. D., 1981. Volume of fluid (VOF) method for the dynamics of free boundaries. Journal of Computational Physics, 39(1), 201-225.

Huang Z., He F., Zhang W., 2014. A floating box-type breakwater with slotted barriers. Journal of Hydraulic Research. 52(5), 720-727.

Kou Y., Xiao L., Liu J.H., Yang L.J., 2016. Experimental research on the wave-breaking chambers of very large floating offshore base. Journal of Ship Mechanics, 20(07),

833-840.

Koley, S., 2020. Water wave scattering by floating flexible porous plate over variable bathymetry regions. Ocean Engineering, 214, 107686.

Lee J.I., Kim Y.T., and Shin S.,2014. Experimental studies on wave interactions of partially perforated wall under obliquely incident waves. The Scientific World Journal, 954174.

Li Y. and Teng B., 2015. Wave Action on Maritime Structures. China Ocean Press, Beijing.

Liu J., Lin G., Li J., 2012. Short-crested waves interaction with a concentric cylindrical structure with double-layered perforated walls. Ocean Engineering, 40, 76-90.

Liu P., Lin, P., Chang, K., Sakakiyama, T., 1999. Numerical Modeling of Wave Interaction with Porous Structures. Journal of Waterway, Port, Coastal, and Ocean Engineering, ASCE, 125, 322-330.

Liu Y., Li H.J., 2014. Wave scattering by dual submerged horizontal porous plates: Further results. Ocean Engineering, 81, 158-163.

Mackay E., Johanning L., 2020. Comparison of analytical and numerical solutions for wave interaction with a vertical porous barrier. Ocean Engineering, 199, 107032.

Mackay, E., Johanning, L., Qiao, D., Ning, D., 2019. Numerical and experimental modelling of wave loads on thin porous sheets. Proceedings of the 38th International Conference on Ocean, Offshore and Arctic Engineering, OMAE, 2019-95148.

Madsen, P.A., 1983. Wave reflection from a vertical permeable wave absorber. Coastal Engineering, 7, 381–396.

McIver, P., 1998. The blockage coefficient for a rectangular duct containing a barrier with a circular aperture. Applied Ocean Research, 20, 173-178.

Mei, C., Liu, P., Ippen, A., 1974. Quadratic loss and scattering of long waves. Journal of Waterway, Port, Coastal and Ocean Engineering, 100, 217-239.

Mohapatra S. C., Soares C. G., 2020. Hydroelastic response of a flexible submerged porous plate for wave energy absorption. Journal of Marine Science and Engineering, 8(9), 698.

Molines, J., Bayón, A., Gómez-Martín, M. E., Medina, J. R., 2020. Numerical Study of Wave Forces on Crown Walls of Mound Breakwaters with Parapets. Journal of Marine Science and Engineering, 8(4), 276.

Molin B., 2011. Hydrodynamic modeling of perforated structures. Applied Ocean

Research, 33(1), 1-11.

Na'im I., Shahrizal A. Safari M., 2018. A Short Review of Submerged Breakwaters, MATEC Web of Conferences, 203: 01005.

Qiao D., Feng C., Yan J., Liang H., Ning D., Li B., 2020. Numerical simulation and experimental analysis of wave interaction with a porous plate. Ocean Engineering, 218, 108106.

Polubarinova-Kochina, P., 1962. Theory of ground water movement. Princeton University Press, Princeton.

Ren X. and Ma Y., 2015. Numerical simulations for nonlinear waves interaction with multiple perforated quasi-ellipse caissons. Mathematical Problems in Engineering Theory Methods & Applications, 895673.

Smith M. J. A., Peter M. A., Abrahams I. D. and Meylan M. H., 2020. On the Wiener-Hopf solution of water-wave interaction with a submerged elastic or poroelastic plate. Proceedings of the Royal Society A, 476, 20200360.

Sankarbabu K., Sannasiraj S. A., Sundar V., 2008. Hydrodynamic performance of a dual cylindrical caisson breakwater. Coastal Engineering, 55(6), 431-446.

Sollitt C. K. and Cross R. H., 1972. Wave Transmission through Porous Breakwaters. In: Proceedings of 13th Conference on Coastal Engineering, ASCE, 3, 1827-1846.

Teng B., Zhang X., Ning D., 2004. Interaction of oblique waves with infinite number of perforated caissons. Ocean Engineering, 31, 615-632.

Wu Y., Yeh C., Hsiao S., 2014. Three-dimensional numerical simulation on the interaction of solitary waves and porous breakwaters. Coastal Engineering, 85, 12-29.

Yueh C. Y., Chuang S. H., 2009. The reflection of normal incident waves by absorbing-type breakwaters. China Ocean Engineering, 23, 729-740.

Zheng S. M., Meylan M. H., Fan L., Greaves D., Iglesias G., 2020a. Wave scattering by a floating porous elastic plate of arbitrary shape: A semi-analytical study. Journal of Fluids and Structures, 92, UNSP, 102827.

Zheng S. M., Meylan M. H., Greaves D., Iglesias G., 2020b. Water-wave interaction with submerged porous elastic disks. Physics of Fluids, 32(4), 047106.

Zheng S. M., Meylan M. H., Zhu G., Greaves D., Iglesias G., 2020c. Hydroelastic interaction between water waves and an array of circular floating porous elastic plates. Journal of Fluid Mechanics, 900.

Numerical Analysis on Wave Load Reduction Effect of a Solid Wall with Porous Plate by Macroscopic CFD Approach

Dongsheng Qiao[1], Jun Yan[1*], Changlong Feng[1, 2], Haizhi Liang[3], Dezhi Ning[1**], Binbin Li[4], Lars Johanning[5]

1. State Key Laboratory of Coastal and Offshore Engineering, Dalian University of Technology, Dalian 116024, China;
2. CCCC Water Transportation Consultants Co. Ltd. Qingdao Branch, Qingdao 266071, China;
3. School of Civil Engineering, Qingdao University of Technology, Qingdao 266033, China;
4. Shenzhen International Graduate School, Tsinghua University, Shenzhen 518055, China;
5. Renewable Energy Group, CEMPS, University of Exeter, Penryn Campus, Penryn, Cornwall TR10 9FE, UK.

Abstract: The porous structures are widely designed in coastal and ocean engineering to reduce the wave load. A macroscopic CFD approach is established to study the wave interaction with a porous plate placed in front of a solid wall. The established numerical wave tank was firstly validated by the analytical results of a vertical wall, and the macroscopic CFD model was validated by the experimental results of a single vertical porous plate. Then the wave load reduction effect of a solid wall with a vertical porous plate in front is investigated, the influences of porosity and relative gap width are compared, and the effects of wave height are also analyzed. The results demonstrate that the porosity and relative gap width are the main effect factors to the wave force reduction effect, and the wave forces on structure increase almost linearly with the increase of relative wave height, while the wave load reduction coefficient and refection coefficient are not linearly. A porosity of 0.2 and relative gap width of 0.2~0.3 are deemed to be optimal geometry parameters at which the wave load reduction effect is optimal. The total horizontal wave force increases nonlinearly with the increase of wave heights, and the quadratic pressure drop condition is essential when studying the wave force on thin porous structures.

Keywords: Porous plate; offshore structures; wave load; CFD simulation; macroscopic approach.

* Corresponding author. Email address: junyan@dlut.edu.cn;

** Corresponding author. Email address: dzning@dlut.edu.cn.

1. Introduction

The wave loads are usually the dominant loads in the design of ocean engineering structures when suffering from the complex ocean environmental loads. With the rapidly development of ocean engineering construction, the investigations on reducing wave force of ocean engineering structures are of great importance. The porous structures, such as the rubble mound breakwater (Andersen et al., 2011), slotted floating box-type breakwaters (Huang et al., 2014), fixed permeable caisson breakwaters (Yueh and Chuang, 2009), submerged porous breakwaters (Na'im et al., 2018), and wave absorbing chambers of floating offshore base (Kou et al., 2016), have been applied in the coastal and ocean engineering structures to absorb wave impact and protecting structures, and the investigations on the interaction between waves and porous structures are one of the key design issues.

Using wave tank test to investigate the interaction between waves and porous structures have been conducted by many scholars. A large-scale model test was carried out by Bergmann and Oumeraci (1998) in the wave tank, and the wave pressure distribution on the porous walls was investigated. Chen et al. (2002) carried out a series of regular wave experiments on perforated caisson in the wave tank and studied the relationships between the reflection coefficient and the structure sizes, including the relative width of the wave absorbing chamber, the porosity, and the relative wave height. Ajiwibow (2011) conducted a 2-D model test to measure the effectiveness of perforated skirt breakwater for short-period waves and analyzed the relationship between the transmission coefficient and non-dimensional variables (skirt draft/incident wave height). A 3-D tank test was performed by Lee et al. (2014) to study the wave heights distribution in terms of evolution phenomena on partially perforated walls, and it was observed that the perforation could reduce wave heights effectively and the perforated wall with side walls performed better on wave height reduction. Liu and Li (2014) conducted experiments to investigate the wave scattering by two-layer horizontal porous plates. Chyon et al. (2017) investigated the interaction between wave and horizontal slotted submerged breakwater by experiments and the effect of size and porosity of the structure on the reduction of wave height. Fang et al. (2018) proposed a four-layer submerged horizontal porous plate breakwater and also discussed the design of the geometrical parameters by 2-D model tests in the wave tank. Through an experimental study on the interaction between solitary waves and vertical porous plates,

Francis et al. (2020) investigated the porosity effect on the dissipation of wave energy and found that the plate porosity ranging 0.1~0.2 gave the optimal energy dissipation.

The tank tests are usually limited by the experimental conditions, such as the secondary refection effect of wave-maker boundary and the accuracy of wave probes and force sensors, and the scale effects also need to be considered. Some investigations concentrated on developing analytical solutions of the interaction of wave-porous structures. For the fluid motion in the porous media, Sollit and Cross (1972) gave a governing equation utilizing the characteristic function expansion method. Dalrymple et al. (1991) systematically studied the reflection and propagation of oblique waves impacting on the porous structures. Teng et al. (2004) studied the interaction between oblique waves and perforated caisson based on the potential flow theory by using characteristic function expansion method, and the variation laws of reflection coefficient and wave force with the incident angle and hole size were also analyzed. Sankarbabu et al. (2008) theoretically investigated the hydrodynamic performance of a breakwater formed by a row of dual cylindrical caisson with a porous outer cylinder, by using a modified characteristic function expansion method. For multi-layers porous plates, Geng et al. (2018) investigated the wave absorbing efficiency based on the linear potential flow theory, and the effects of thickness, porosity, and layout form of plates on wave absorption were also analyzed. Mackay and Johanning (2020) compared two analytical solutions of the interaction between wave and a vertical porous plate, which are derived by two different methods for taking the depth-average of the pressure drop across the porous barrier and neglect the evanescent modes in the wave field. By comparing with the results of Boundary Element Method (BEM) modeling, the two analytical solutions were confirmed to reliable for predicting the wave force on the plate and the transmission and reflection coefficients. Zheng et al. (2020a, 2020b, 2020c) and Koley et al. (2020) developed a semi-analytical model using the linear potential flow theory to investigate the wave scattering of various kinds of porous elastic plates in different water depth conditions. Smith et al. (2020) studied the water-wave scattering by a semi-infinite submerged thin elastic plate using the Wiener-Hopf technique. Mohapatra and Soares (2020) studied the hydroelastic response of a flexible submerged porous plate using the generalized expansion formula based on Green's function.

When the geometry of the physical problem becomes more complicated, the analytical approaches become increasingly difficult. Thus, using numerical approaches

based on the potential theory are widely applied. Liu et al. (2012) proposed a semi-analytical scaled boundary finite element method (SBFEM) to study the interaction between short-crested wave and a concentric cylindrical structure with double-layered perforated walls, and discussed the effects of wave conditions and geometry parameters of the structure on wave force and water surface elevations. Mackay et al. (2019) established an iterative BEM model to solve the quadratic pressure loss across the porous sheet and validated it by comparing the tank tests. Meanwhile, some investigations on the interaction between waves and porous structures were also conducted by the CFD method. Ren and Ma (2015) used the CFD method to establish a 3-D numerical wave tank (NWT) and simulated the interaction between nonlinear waves and perforated quasi-ellipse caissons. It was observed that with the wave period decreased, the wave force on caissons would be diminished, and a smaller transverse distance among caissons would result in higher wave forces. Chen et al. (2019) used Ansys Fluent to create a 2-D NWT and performed simulations on the interaction between waves and a vertical porous wall placed in solid wall front. The effects of gap width and porosity on wave force and reflection coefficient were analyzed.

The potential theory usually cannot well capture the viscous effect, and the CFD investigations listed above usually need a huge number of mesh cells and take a lot of computing time, with the reason of high-quality grids requirement for the fluid field, especially near the boundaries of porous structures. Alternatively, without explicitly establishing the geometric model of porous structures to simulate the microscopic processes of waves and porous structures interaction, the macroscopic mesh-free approaches which is more concerned on the macroscopic effects of the porous structure on incident waves have been proposed. Liu et al. (1999) developed a numerical model to simulate the wave-porous structures interaction, in which the spatially averaged Navier-Stokes equations were applied to describe the flow in porous media, and the empirical linear and nonlinear frictional forms were used to model the drag forces produced by the solid skeleton. The proposed model was applied to analyze the flow passing through a porous dam and the breaking wave overtopping a caisson breakwater protected by porous armor units. A similar CFD model was proposed by del Jesus (2012) for heterogeneous media where porosity varies along the porous body, with three terms that describe the physical process of water flow interacting with porous structures covered in the momentum equations. By comparing the simulated results with

experiments, the proposed model was verified to be reliable. Based on the work of del Jesus, Higuera et al. (2014) established a CFD model for wave/flow-porous structures interaction using OpenFOAM, by analyzing the pressure loss of flows passing through porous structures and adding the pressure loss term into the momentum equation of the porous media region. The established model was applied to porous dam break and the interaction between waves and rubble breakwater, and the comparison with experiments indicated that the established CFD by this macroscopic approach is reasonable. A 3-D large-eddy-simulation model with macroscopic model equations of porous flow was proposed by Wu et al. (2014), and the interaction between solitary waves and permeable breakwaters was studied. It was demonstrated that the results obtained by microscopic and macroscopic modeling both consistent with experiments in terms of water surface elevations and velocity fields. Molines et al. (2020) established a CFD model for the simulation of wave attacking mound breakwaters with parapets by OpenFOAM, where the porous media was modeled by a macroscopic approach. The established model was validated by experiments and then a series of numerical simulation were conducted by the CFD model for evaluating the effects of nine crown wall geometries with and without parapets. Qiao et al. (2020) established a CFD model with quadratic pressure drop condition for simulating the wave interaction with thin porous plate, and the comparison with experimental results shown that the alternative CFD method is feasible. The CFD models above using macroscopic approaches avoided dealing with the complex physical boundary conditions and thus decreasing the mesh numbers. The accuracy is confirmed to be sufficient for predicting the wave force on porous structures and wave surface elevations.

The porous plate or wall is widely used in offshore structures against wave attack, and the wave force reduction effect of a porous plate on offshore structures needs to be further investigated. Based on the research of wave interaction with only a porous plate by the authors (Qiao et al., 2020), a solid vertical wall with a porous plate in front is further investigated in this paper. A NWT is created by ANSYS Fluent, and a macroscopic approach is applied to establish the numerical model for simulating the interaction between waves and vertical porous plate. The established numerical model is firstly applied to the case of interaction between waves and a vertical porous plate. The numerical results are compared with a microscopic approach and model tests, and excellent agreement is obtained. Then the established CFD model is applied to simulate

the interaction between waves and the structure of a solid vertical wall with a porous plate in front. The wave force on the structure and the reflection coefficient are studied with different porosities of porous plate and relative gap width between the porous plate and solid wall.

This paper is organized as follows. The establishment of the NWT and macroscopic pressure loss model of porous plate is presented in Section 2. Section 3 presents the established model validation, including the mesh convergence validation, a case validation for NWT, and a case validation of a vertical porous plate. The CFD simulations and analysis of wave interaction with SWP are presented in section 4. Finally, the conclusions are presented in Section 5.

2. Numerical model

2.1. Governing equations

The Navier-Stokes equations of general form are used to describe the flow in NWT:

$$\frac{\partial u}{\partial x}+\frac{\partial v}{\partial y}=0 \tag{1}$$

$$\frac{\partial u}{\partial t}+u\frac{\partial u}{\partial x}+v\frac{\partial u}{\partial y}+w\frac{\partial u}{\partial z}=-\frac{1}{\rho}\frac{\partial p}{\partial x}+\nu\left(\frac{\partial^2 u}{\partial x^2}+\frac{\partial^2 u}{\partial y^2}+\frac{\partial^2 u}{\partial z^2}\right) \tag{2}$$

$$\frac{\partial v}{\partial t}+u\frac{\partial v}{\partial x}+v\frac{\partial v}{\partial y}+w\frac{\partial v}{\partial z}=-\frac{1}{\rho}\frac{\partial p}{\partial y}+\nu\left(\frac{\partial^2 v}{\partial x^2}+\frac{\partial^2 v}{\partial y^2}+\frac{\partial^2 v}{\partial z^2}\right) \tag{3}$$

$$\frac{\partial w}{\partial t}+u\frac{\partial w}{\partial x}+v\frac{\partial w}{\partial y}+w\frac{\partial w}{\partial z}=-\frac{1}{\rho}\frac{\partial p}{\partial z}+\nu\left(\frac{\partial^2 w}{\partial x^2}+\frac{\partial^2 w}{\partial y^2}+\frac{\partial^2 w}{\partial z^2}\right)-g \tag{4}$$

where, u, v and w are the instantaneous velocity; p represents the instantaneous effective pressure; ν is the molecular viscosity. The free water surface in NWT is captured by the VOF (volume of fluid) method (Hirt and Nichols, 1981), and for each control volume, the volume fraction of air and water phases can be described by following equations:

$$\frac{\partial F_i}{\partial t}+F_i\left(\frac{\partial u}{\partial x}+\frac{\partial v}{\partial y}+\frac{\partial w}{\partial z}\right)=0 \tag{5}$$

$$\sum_{i=1}^{2}F_i=1 \tag{6}$$

where, F_i represents the volume fraction of the ith phase.

2.2. Wave generation and absorption

Figure 1 shows the empty NWT, which can generate expected waves on the left boundary and eliminate waves with the wave absorbing region at the end. In this paper, a finite volume method (FVM)-based CFD software, ANSYS Fluent, is used to establish the NWT. A pushing-board method is applied to generate expected regular linear waves in the left boundary of NWT, and following equations can describe the motion of pushing-board:

$$x_b(t) = \frac{S_0}{2}\sin \omega t \tag{7}$$

$$u_b(t) = \frac{\omega S_0}{2}\cos \omega t \tag{8}$$

where, t is the flow time; $x_b(t)$ and $u_b(t)$ represent the displacement and velocity of pushing-board respectively; ω is the wave frequency; S_0 is the stroke of pushing-board, which is related to the parameters of the expected wave. The surface elevation of wave generated by pushing-board can be expressed as equation (9) (Li and Teng, 2015), from which the relationship between S_0 and the parameters of the expected wave can be obtained as equation (10):

$$\eta(x,t) = \frac{S_0}{2}\frac{4\sinh^2(kd)}{2kd + \sinh(2kd)}\cos(kx - \omega t) = \frac{H}{2}\cos(kx - \omega t) \tag{9}$$

$$S_0 = \frac{2kd + \sinh(2kd)}{4\sinh^2(kd)}H \tag{10}$$

where, η represents the wave surface elevation; k represents the wave number; d represents the water depth; H represents the wave height. The velocity of the pushing-board is controlled as equation (8) by Users Define Function (UDF) of Fluent, and then the wave can be generated as equation (9) expressing.

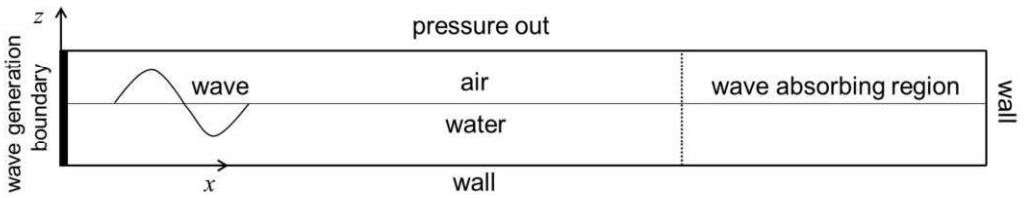

Fig. 1 Numerical wave tank (NWT)

A wave absorbing region is set at the end of the tank to eliminate the reflection wave, where the linearly increasing damping is applied, and the damping source terms are added into the momentum equations. The momentum equations with added

damping source terms can be expressed as (Madsen, 1983):

$$\frac{\partial u}{\partial t}+u\frac{\partial u}{\partial x}+v\frac{\partial u}{\partial y}+w\frac{\partial u}{\partial z}=-\frac{1}{\rho}\frac{\partial p}{\partial x}+\nu(\frac{\partial^2 u}{\partial x^2}+\frac{\partial^2 u}{\partial y^2}+\frac{\partial^2 u}{\partial z^2})-\mu(x)u \tag{11}$$

$$\frac{\partial v}{\partial t}+u\frac{\partial v}{\partial x}+v\frac{\partial v}{\partial y}+w\frac{\partial v}{\partial z}=-\frac{1}{\rho}\frac{\partial p}{\partial y}+\nu(\frac{\partial^2 v}{\partial x^2}+\frac{\partial^2 v}{\partial y^2}+\frac{\partial^2 v}{\partial z^2})-\mu(x)v \tag{12}$$

$$\frac{\partial w}{\partial t}+u\frac{\partial w}{\partial x}+v\frac{\partial w}{\partial y}+w\frac{\partial w}{\partial z}=-\frac{1}{\rho}\frac{\partial p}{\partial z}+\nu(\frac{\partial^2 w}{\partial x^2}+\frac{\partial^2 w}{\partial y^2}+\frac{\partial^2 w}{\partial z^2})-g-\mu(x)w$$

where, the damping coefficient $\mu(x)$ is expressed as:

$$\mu(x)=\begin{cases}0 & ,\ for\ x\le x_1\ or\ x\ge x_2\\ \alpha\dfrac{(x-x_1)}{(x_2-x_1)} & ,\ for\ x_1<x<x_2\end{cases} \tag{13}$$

where, x_1 and x_2 are the start and end of wave absorbing region; α is an empirical coefficient, which is set as 8.0 in this paper.

2.3. Porosity implementation

As stated in Section 1, compared to the microscopic CFD approach, the macroscopic CFD approach not only can avoid huge computational cost but also have sufficient accuracy for simulating wave-porous structures interactions. The macroscopic porosity effect can be represented by an averaged pressure loss through the porous media (Mackay and Johanning, 2020), where the detailed geometry does not need to be resolved explicitly. This subsection will analyze the pressure loss of interaction between waves and vertical porous plate.

Darcy (1856) found that when water flowing through sand, the hydraulic gradient can be assumed to be linearly proportional to the flow passing through, as shown in the flowing equation:

$$I=-\frac{1}{\rho g}\frac{\partial p}{\partial y}=a_p\bar{u} \tag{14}$$

where, I is the hydraulic gradient, a_p is an empirical coefficient. $\bar{u}$ is averaged discharge velocity. In the work of Forcheimer (1901), more energetic flows with high Reynolds number were considered, and Darcy's law was thus extended by adding a quadratic term:

$$I=-\frac{1}{\rho g}\frac{\partial p}{\partial y}=a_p\bar{u}+b_p\bar{u}|\bar{u}| \tag{15}$$

where, b_p is an empirical coefficient. Polubarinova-Kochina (1962) considered the added mass effects of unsteady flows and added the transient term into the formulation:

$$I = -\frac{1}{\rho g}\frac{\partial p}{\partial y} = a_p \bar{u} + b_p \bar{u}|\bar{u}| + c_p \frac{\partial \bar{u}}{\partial t} \tag{16}$$

where, c_p is an empirical coefficient. Sollitt and Cross (1972) further proposed that when a wave passing through a vertical thin porous barrier, the pressure loss ΔP can be expressed as:

$$\frac{\Delta P}{\rho} = \frac{\nu \boldsymbol{U}}{l} + \frac{C_f}{2}\boldsymbol{U}|\boldsymbol{U}| + c\frac{\partial \boldsymbol{U}}{\partial t} \tag{17}$$

where, ν is the molecular viscosity; l is a length scale, which is related to geometry characteristics of porous structures; c is an inertial coefficient; $\boldsymbol{U}$ represents the velocity normal to the plate; C_f is a dimensionless friction coefficient, which can be expressed as (Molin, 2011):

$$C_f = \frac{1-\varepsilon}{\varepsilon^2 \delta} \tag{18}$$

where, ε represents the porosity of porous plate; δ is the discharge coefficient, usually taken as 0.4–0.5 (Mackay and Johanning, 2020), and it is chosen as 0.5 in this paper. The first term in the right of equation (16) is a linear viscous friction term, the second term is a quadratic turbulent dissipation term, and the third term is a inertia term. The linear viscous friction term is dominant at low Reynolds number while the quadratic turbulent dissipation term becomes dominant at high Reynolds number (Sollitt and Cross, 1972). The Reynolds numbers for wave interaction with thin porous plates are usually sufficiently high so that the linear viscous friction term can be neglected (Mackay and Johanning, 2020). The inertia term accounts for added mass effects and transient interaction between the fluid and porous structures. The inertial coefficient c is related to the geometries of porous structures. For a porous plate with circle holes, the inertial coefficient c can be calculated by the following equation (McIver, 1998):

$$\frac{c}{s} \approx 0.3898\varepsilon - 0.03239\sqrt{\varepsilon} + 1.2415 + \frac{0.8862}{\sqrt{\varepsilon}} \tag{19}$$

where, s represents the distance between adjacent hole centers.

To model wave flow passing through the porous plate, the pressure loss per unit

thickness is added into the horizontal momentum equation in the geometric region of porous plate as a source term. According to equations (17) and (18), the added source term S_{porous} can be expressed as:

$$S_{porous} = -\frac{1}{\rho}\frac{\Delta P}{\Delta n} = -\frac{1}{\Delta n}\left(\frac{1-\varepsilon}{2\varepsilon^2\delta}u|u| + c\frac{\partial u}{\partial t}\right) \tag{20}$$

where, Δn is the thickness of porous plate.

3. Numerical model validation

3.1. Mesh convergence validation

Figure 2 shows the generated mesh of an empty NWT. In *x*-direction, the mesh size is defined to 1/10 of S_0 in the moving region of pushing-board, Δx in the wave propagation region, and changes to sparse gradually in the wave absorbing region. In y-direction, the mesh size is defined to Δy in the one wave height region, and changes to sparse gradually in the remaining region.

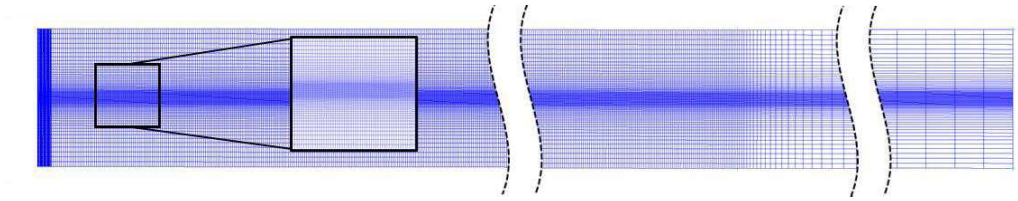

Fig. 2 Mesh refinement

For mesh convergence validation, four mesh types are considered as Table 1 shown. The same wave condition (T=1.9s, H=0.0772m, d=1.0m, L=4.85m) is generated in the NWT under different mesh characteristics. After comparing the wave surface elevations under four different mesh types with the theoretical solution, the mesh type 2 where $\Delta y = 1/10H$, $\Delta x = 1/160L$ is selected due to its enough high simulation precision and a relatively smaller number of mesh cells.

Tab. 1 Results of simulated wave height under different mesh types

Mesh type	mesh1	mesh2	mesh3	mesh4
H/Δy	5	10	15	20
λ/Δx	80	160	240	320
Δy(m)	0.0154	0.0077	0.0051	0.0039
Δy (m)	0.0606	0.0303	0.0202	0.0152
wave height (m)	0.0763	0.0768	0.0768	0.0769
relative tolerance	-1.15%	-0.52%	-0.43%	-0.39%

3.2. Model Validation: a vertical wall

A solid vertical wall occupying the full water column is conducted to validate the established NWT. As shown in Figure 3, the solid wall with 1.5m height is set at 25m from the wave-making board. The mesh refinement is shown in Figure 4, which is the same as the empty NWT in Figure 2, except for the mesh cells nearby the solid wall which are further defined as 1/10 of the wall thickness. A regular wave with H =0.0772m, T =1.9s, d =1.0m is generated in the NWT.

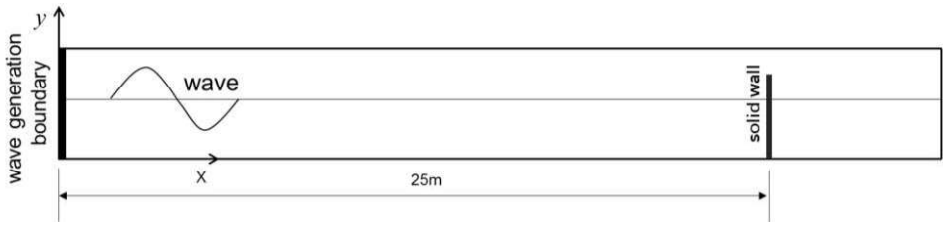

Fig. 3 The layout of NWT with vertical solid wall

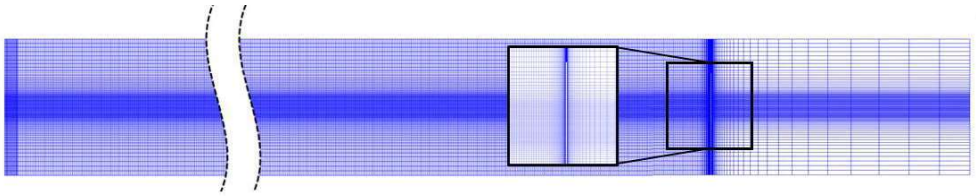

Fig. 4 Generated mesh of NWT with a solid vertical wall

It is known that a standing wave occurs when a regular wave reflected by a vertical wall. Figure 5 shows the time series of water surface elevation at the vertical solid wall. It can be obtained that the average wave height is 1.538m, only 0.38% differing from the analytical value, which is equal to two times of the incident wave height. Figure 6 shows the time series of horizontal wave force on the vertical solid wall, and it can be obtained that the average maximum wave force is 508.82N. The analytical solution of the wave force on the vertical solid wall can be obtained by integrated the pressure on the wall along with the water depth, which can be calculated by following equations (Li and Teng, 2015):

$$p(z) = \rho g H \frac{\cosh k(z+d)}{\cosh kd} \tag{21}$$

$$f = \int_d^\eta p(z)dz = \int_d^0 \rho g H \frac{\cosh k(z+d)}{\cosh kd} dz + O(\varepsilon^2) \approx \frac{\rho g H}{k} \tanh kd \tag{22}$$

where, $p(z)$ is the relative pressure on the solid wall along with the depth; f is horizontal wave force on the wall. It can be obtained that the analytical wave force on the wall is 502.11N, and the numerical wave force is only 1.34% differing from the

analytical values. The results above have validated that the established NWT is reliable.

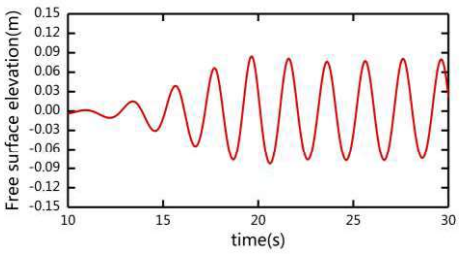

Fig. 5 Time series of free surface elevation at x=25m

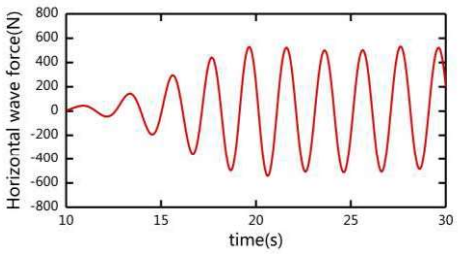

Fig. 6 Time series of horizontal wave force on the solid wall

3.3. Model Validation: a single porous plate

The established CFD model using the macroscopic approach is firstly applied to the wave interaction with a vertical porous plate for validation. The presented model is respectively compared with a microscopic approach and model tests.

3.3.1. Comparison with a microscopic approach

Figure 7 shows the layout of the NWT with a porous plate under the presented macroscopic CFD model. Figure 8 shows the generated mesh, which is the same as the empty NWT in Figure 2 except for the mesh of porous layer being refined as 1/10 of the porous thickness and the nearby mesh being refined correspondingly. The used porous plate in this subsection is 1.5m in height, 1.0m in width, and 1cm in thickness, and the porosity is 0.3. The corresponding CFD simulation under the microscopic approach is conducted with a 3-D model, and the layout of NWT is the same as Figure 7. Figure 9 simply shows the porous plate used in the microscopic approach, where the interval of circular holes s=25mm and radius r=7.73mm, thus the porosity also being 0.3. The generated mesh of NWT is also the same as Figure 8, except for the mesh nearby the porous plate being refined as Figure 10 shown. A regular wave condition of H=0.0772m, T=1.9s, d=1.0m is generated in the NWT, and the wave force on the porous plate is monitored.

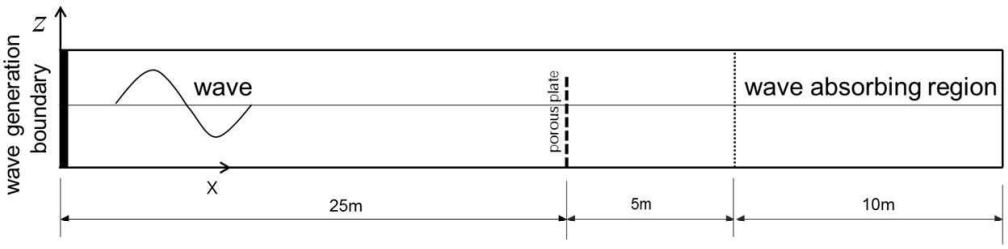

Fig. 7 Layout of NWT with a vertical porous plate

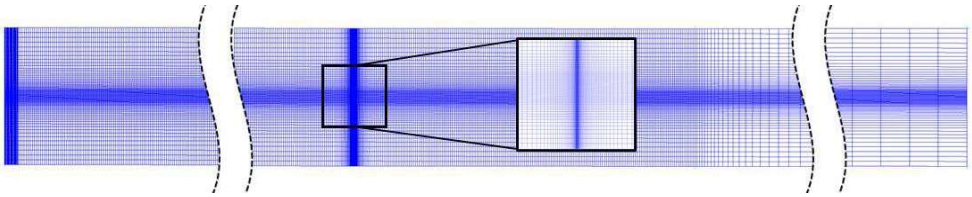

Fig. 8 Generated mesh of NWT with a porous plate under presented CFD model

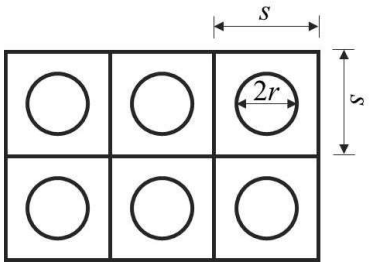

Fig. 9 Illustration of a regular grid of holes in porous plates

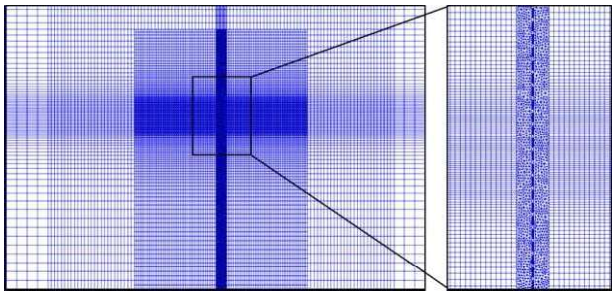

Fig. 10 Generated mesh nearby the porous plate under microscopic approach

Figure 11 shows the comparison of the monitored horizontal wave force between the two approaches. It can be seen that the wave force on the porous plate calculated by the presented macroscopic CFD model is a little larger than the microscopic approach. However, the difference is very small, indicating that the presented macroscopic CFD approach can well substitute the complex microscopic CFD methods in the simulation of wave interaction with a porous plate.

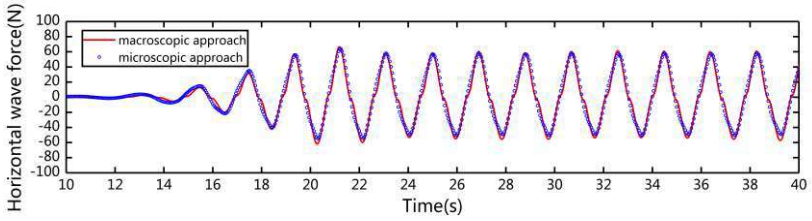

Fig. 11 Time series of horizontal wave force on the porous plate under two CFD approaches

3.3.2. Comparison with model tests

The model tests were conducted at the nonlinear wave flume at Dalian University of Technology (DUT), and the layout in the flume is shown in Figure 12. Two load cells are connected together at the top and bottom sides of the frame to measure the horizontal wave force. A temporarily raised floor was built to install the bottom load cell which is located in a small pit beneath the raised floor. There are five wave probes in total for

monitoring the wave surface elevations. A series of wave conditions with H ranging 0.30~0.772m and T ranging 1.1~1.9s and d=1.0m are applied, and the used porous plate is 1.5m in height, 1m in width, 3mm in thickness and the porosity is 0.2, which also can be simply illustrated as Figure 9. The corresponding CFD simulations using the presented macroscopic model are conducted under the same wave conditions and porous plate parameters, and the layout of NWT is the same as Figure 7, including the same layout of wave probes as model tests.

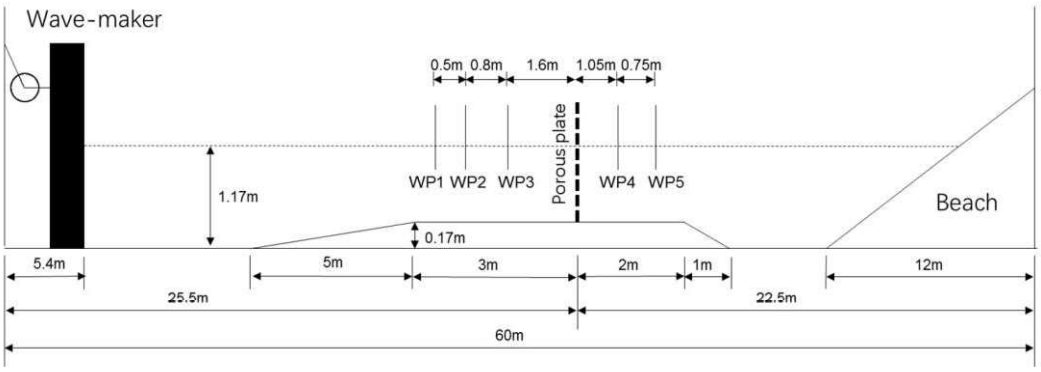

Fig.12 Schematic of the experimental setup in DUT wave flume

Figures 13-14 show the time series of horizontal wave force on the porous plate and the wave surface elevations monitored by wave probes, respectively. Because the distance between wave generated boundary and porous plate are different for CFD simulations and model tests, there is a phase difference between the time series results of two approaches, and the results of model tests are adjusted in phase position for the convenience of comparison. According to Figures 13-14, it can be seen that the CFD results are in good agreement with experiments both in amplitude and phase of horizontal wave force, and the wave surface elevations also show good consistency. The comparing results indicate that the established CFD model is reliable for simulating the interaction between waves and a vertical porous plate.

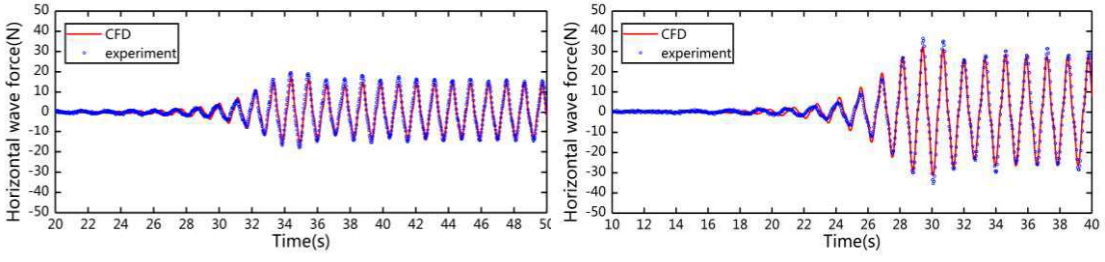

(a) H=0.030m, T=1.1s (b) H=0.0413m, T=1.3s

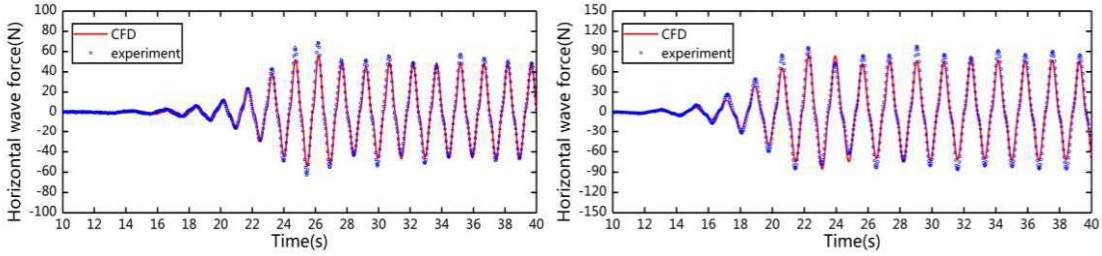

(c) H=0.0533m, T=1.5s (d) H=0.0653m, T=1.7s

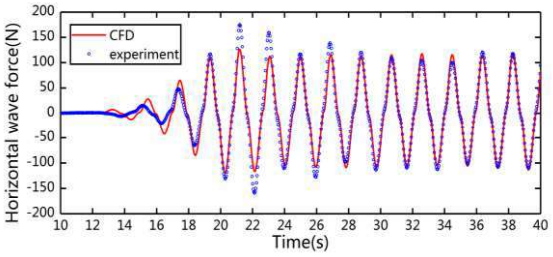

(e) H=0.0772m, T=1.9s

Fig. 13 Time series of horizontal wave force on the porous plate

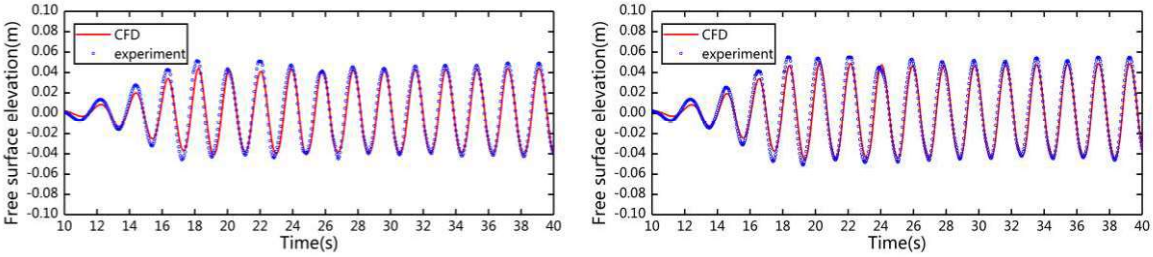

(a) WP1 (b) WP2

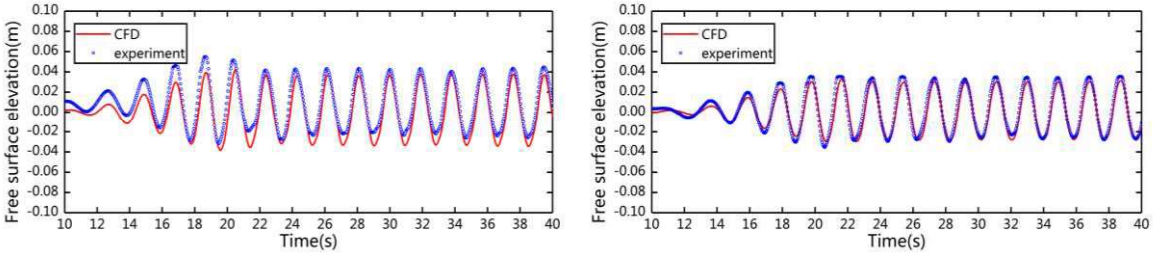

(c) WP3 (d) WP4

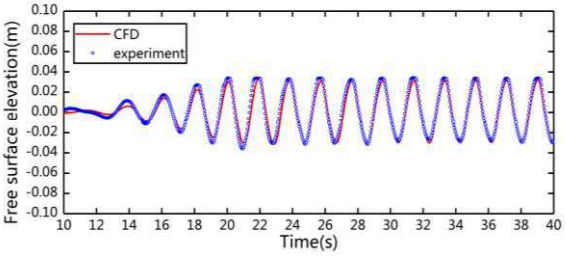

(e) WP5

Fig. 14 Time series of free surface elevations monitored by five wave probes (H=0.0772m, T=1.9s)

4. Simulations results and analysis

The established CFD model is applied to simulate the interaction between waves and the structure of a solid vertical wall with a porous plate in front. The porous plate and solid wall are both 1.5m in height and 1cm in thickness. Figure 15 shows the layout of the NWT with the structure. There are three wave probes set in front of the porous plate for monitoring the reflection waves, and are set as 0.8m, 0.5m, 1.3m apart from each other. The wave forces on the porous plate and solid wall are monitored respectively, and thus the wave force on the whole structure being obtained. Figure 16 shows the generated mesh of NWT including the structure. The wave conditions and model geometry parameters used in this section are shown in Table 2.

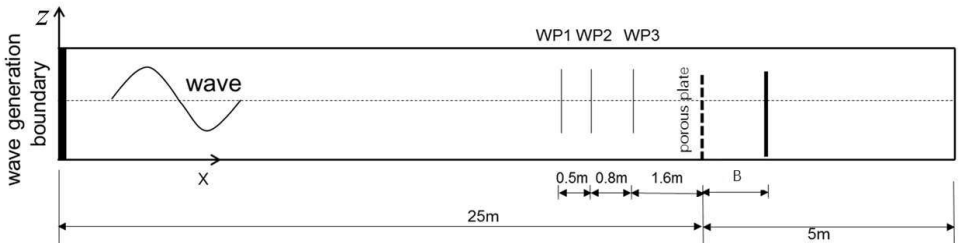

Fig. 15 Layout of NWT including a vertical wall with a porous plate in front

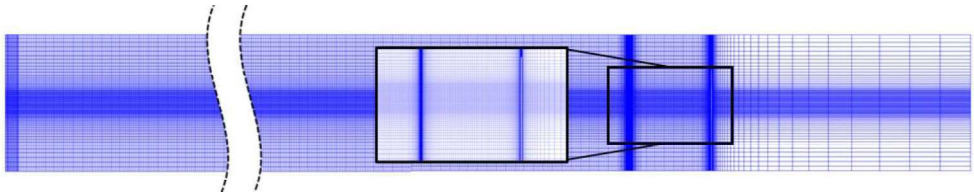

Fig. 16 The generated mesh of NWT including a solid wall with a porous plate in front

Tab. 2 Wave conditions and model geometry parameters

Wave height H (m)	0.16, 0.12, 0.08, 0.04
Wave period T (s)	1.3, 1.5, 1.9, 2.5
Water depth d (m)	1.0
Porosity ε	0.1, 0.2, 0.3, 0.4
Gap width B (m)	0.6, 0.8, 1.0, 1.2

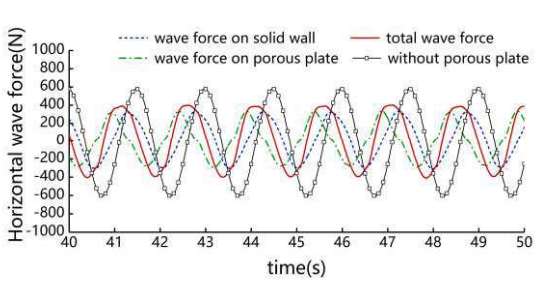

(a) H=0.12m, T=1.5s

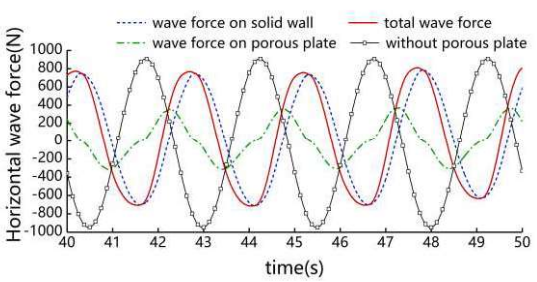

(b) H=0.12m, T=2.5s

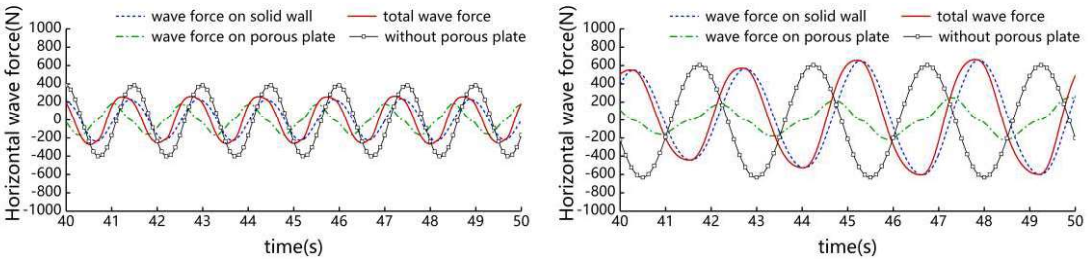

(c) H=0.08m, T=1.5s (d) H=0.08m, T=2.5s

Fig. 17 Time series of horizontal wave force (ε=0.2, B=0.6m)

Figure 17 shows the time series of horizontal wave force on the structure under partial wave conditions with ε=0.2 and B=0.6m. It can be seen that the total wave force on the structure obviously decreases, comparing with the solid wall without a porous plate. It is believed that the decrease is mainly caused by two aspects. Firstly, the porous plate has the impact of dissipating on incident waves, which is mainly related to the porosity. Secondly, there is a phase difference between the wave force on the porous plate and solid wall, which means that partial wave force on the porous plate and solid wall cancels each other out. The phase difference above is mainly related to the gap width B between the porous plate and solid wall, and the wave length L of the incident wave. Therefore, the effects of porosity ε and relative gap width B/L will be analyzed next. For further analysis, the wave force reduction coefficient is introduced to evaluate the wave load reduction effect of the porous plate on the structure, which is defined as the following equation:

$$E_f = \frac{F_{wp} - F_{w0}}{F_{w0}} \tag{23}$$

where, F_{wp} is the wave force on the whole structure with a porous plate and F_{w0} is the wave force on the solid wall without a porous plate. The reflection waves are analyzed at the same time, and the reflection coefficient is defined as:

$$K_r = \frac{H_r}{H_i} \tag{24}$$

where, H_r and H_i are wave heights of reflection and incident wave, respectively. To obtain the reflection wave height, the refection wave and incident wave need to be separated from the wave monitored by wave probes, and the two-point method proposed by Goda and Suzuki (1976) is used.

4.1. Effects of porosity

When an incident wave impacts on the porous plate, some of the wave will be reflected, some will be dissipated, and the remained components will transmit through the porous plate and impact on the solid wall behind. If the porosity is zero, meaning that the porous plate becomes a solid wall, the total wave force will be equal to the wave impacting on a solid vertical wall; in another extreme, if the porosity tends to infinity, meaning that the porous plate does not exist, all components of the incident wave will impact on the solid wall. The maximum total wave force under two extremes above will all approach the largest value. Therefore, an optimal porosity of the porous plate can be expected at which the maximum total wave force being reduced to the smallest value.

Figure 18 shows the time series of total wave force on the structure with different porosities, where the gap width B is fixed as 0.6m. It can be obtained that the amplitude of wave force varies with the porosity of porous plate, meaning that the variation of porosity has a significant effect on the wave force reduction. The effects of porosity on wave force the porous plate and solid wall are shown in Figure 19. It can be obtained that with the increase of porosity, the wave force on porous plate decreases while the wave force on solid wall increases. That is because, with the increase of porosity, the interaction area between wave and porous plate decreases, thus causing the reduction of wave force on it. Meanwhile, more components of incident wave transmit through the porous plate and impact on the solid wall, causing the wave force on it increasing. It also can be inferred from Figure 19 that when the porosity tending to infinity, which means that there is no porous plate and all of the incident wave will impact on the solid wall, the wave force on the porous plate will tend to 0 and the wave force on the solid wall will tend to a constant value, which is approximately equal to the theoretical wave force calculated by equation (23).

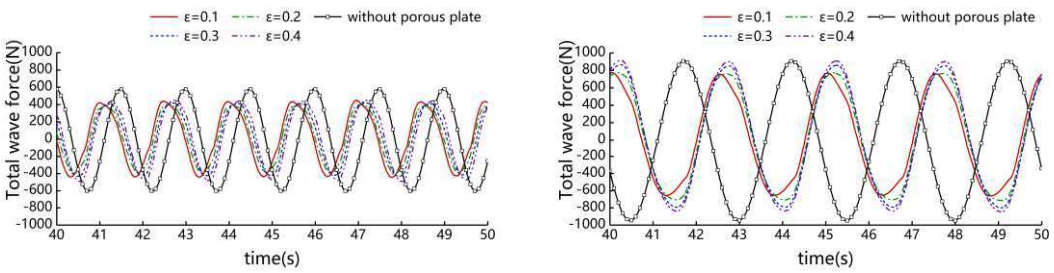

(a) H=0.12m, T=1.5s (b) H=0.12m, T=2.5s

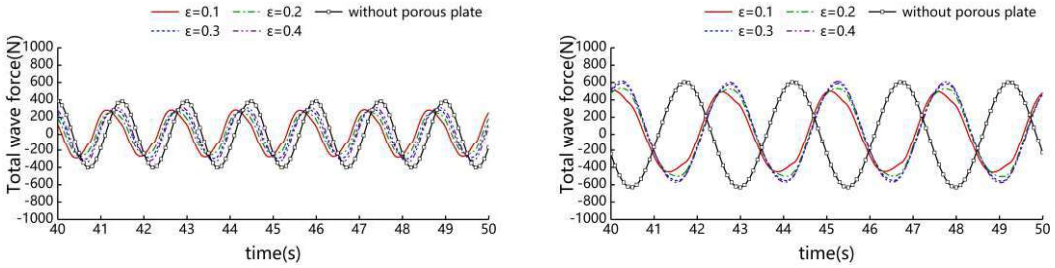

(c) H=0.08m, T=1.5s (d) H=0.08m, T=2.5s

Fig. 18 Time series of total wave force on the structure with different porosities

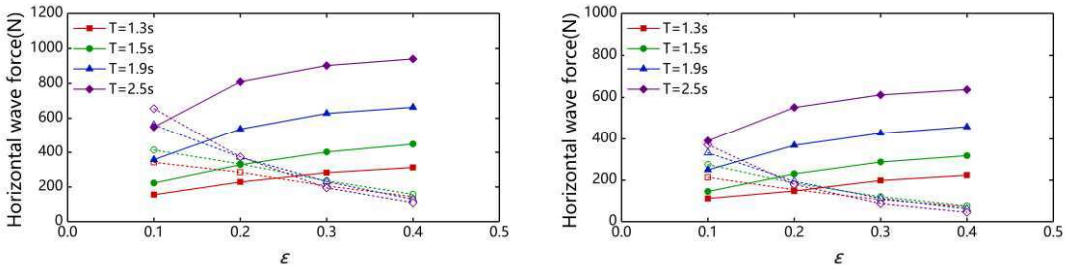

(a) H=0.12m, B=0.6m (b) H=0.08m, B=0.6m

Fig. 19 Maximum wave force on the porous plate and solid wall against ε (dotted lines and hollow marks for the porous plate, solid lines, and marks for the solid wall)

Figures 20-21 show the effect of porosity on E_f and K_r. It is known that, when K_r =1, full-refection occurs and the wave force is the largest; when $K_r < 1$, partial refection occurs, and the smaller K_r will also result in the smaller wave force and the larger E_f. In other words, E_f and K_r are negatively correlated, and it can be seen that the variation laws of E_f and K_r in Figures 20-21 are consistent with the law above. It can be learned from Figure 20 that the variation laws of E_f and porosity under different wave conditions are inconsistent. For most wave conditions, E_f reaches the largest value at ε =0.2, except for the wave conditions of H =0.12m, T =1.3s and H =0.08m, T =1.3s, where E_f reaches the largest value at ε =0.1 and 0.3, respectively.

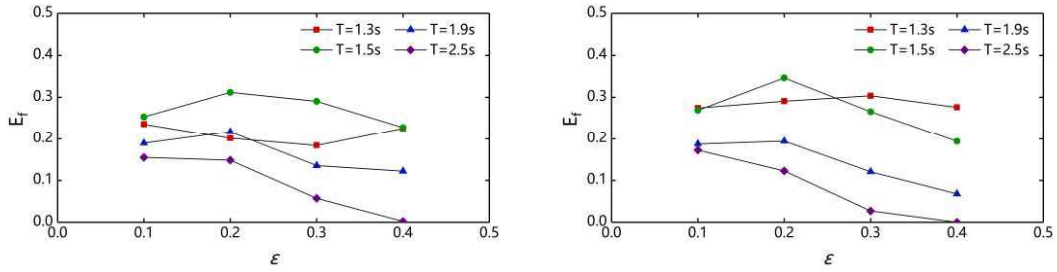

(a) H=0.12m, B=0.6m (b) H=0.08m, B=0.6m

Fig. 20 Effect of porosity on the wave force reduction coefficient

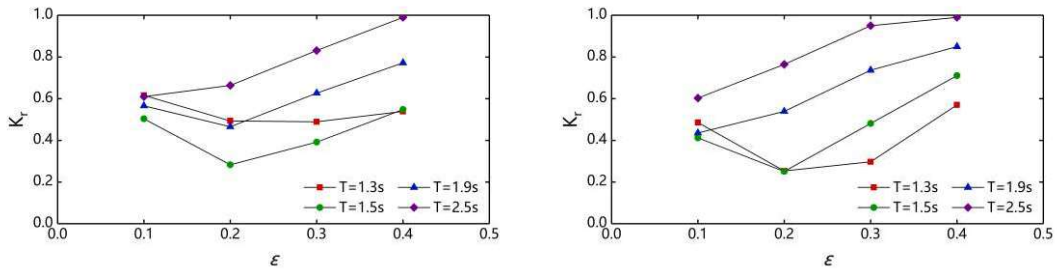

(a) H=0.12m, B=0.6m (b) H=0.08m, B=0.6m

Fig. 21 Effect of porosity on the reflection coefficient

4.2. Effects of relative gap width

The maximum total wave force on the structure is not equal to the sum of maximum wave force on the porous plate and on the solid wall, with the reason of the phase difference between the wave force on them. The phase difference above is related to the gap width B and wave length L. If the porous plate is assumed to have no disturbance on the incident wave, the total wave force on the structure will approach the smallest value when $B/L=0.5$ (or odd times of 0.5). In this case, when the porous plate is impacted by a wave peak, the solid wall is impacted by a wave trough, thus the wave force on the porous plate and solid wall canceling each other out partially, and vice versa. In fact, due to the disturbance of porous plate to the incident wave, the value of B/L at which the total wave force on the structure being the smallest changes. Therefore, an optimal value of B/L ranging 0~0.5 can be expected, at which the total wave force is the smallest under the same conditions. In this subsection, the gap width B is set as 0.6m, 0.8m, 1.0m, 1.2 m, and the corresponding B/L under different wave lengths varies from 0.09 to 0.46. The wave forces on the porous plate, the solid wall, and the whole structure, and the reflection waves under different wave conditions are investigated.

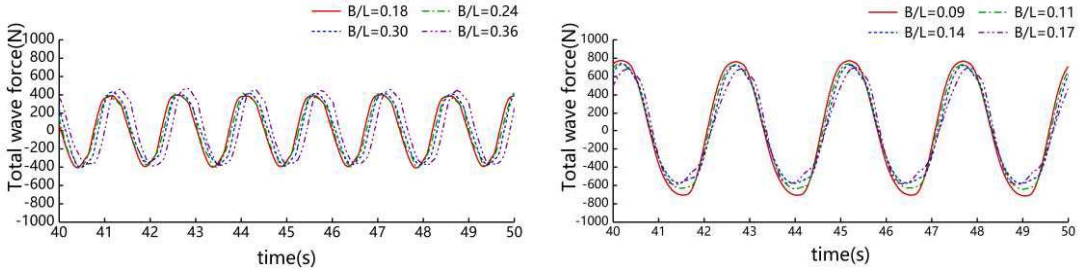

(a) H=0.12m, T=1.5s, ε=0.2 (b) H=0.12m, T=2.5s, ε=0.2

(c) H=0.08m, T=1.5s, ε=0.2 (d) H=0.08m, T=2.5s, ε=0.2

Fig. 22 Time series of total wave force with different B/L

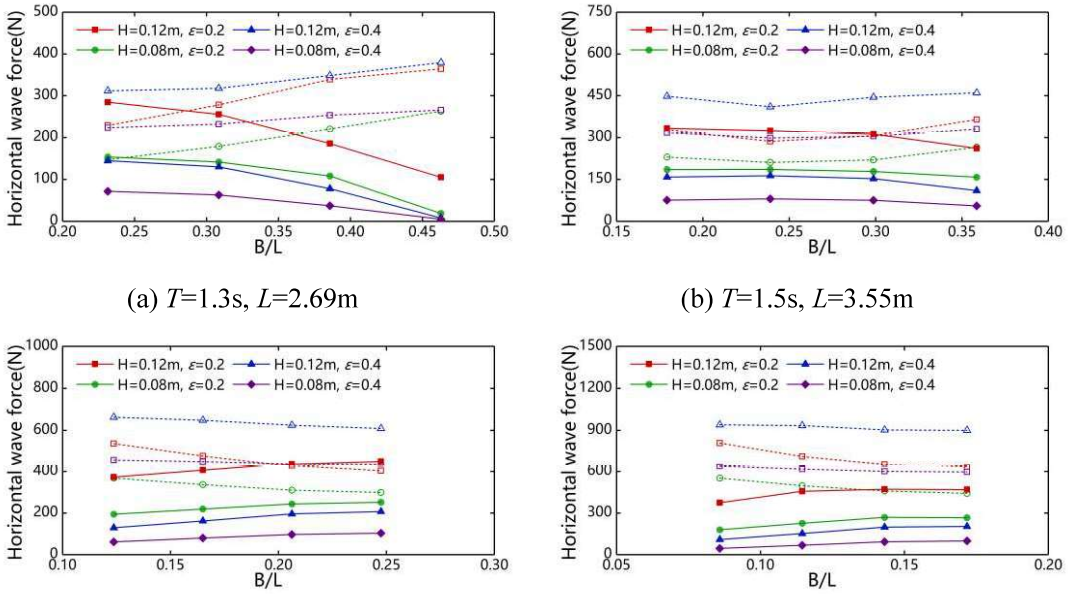

(a) T=1.3s, L=2.69m (b) T=1.5s, L=3.55m

(c) T=1.9s, L=4.85m (d) T=2.5s, L=6.99m

Fig. 23 Maximum horizontal wave force on the porous plate and solid wall against B/L (dotted lines and hollow marks for the porous plate, solid lines and marks for the solid wall)

Figure 22 shows the total wave force on the structure with different relative gap width B/L, and the variation of B/L can cause a reduction of different degrees on total wave force. Figure 23 shows the maximum horizontal wave force on the porous plate and solid wall against B/L. It can be seen that for L=2,69m and 3.55m, where B/L is ranging 0.23~0.46 and 0.18~0.36 respectively, with B/L increases, the wave force on porous plate increases gradually and the wave force on solid wall is opposite;

for $_L$=4.85m and 6.99m, where B/L is ranging 0.12~0.25 and 0.09~0.17 respectively, with B/L increases, the wave force on porous plate decreases gradually and the wave force on solid wall is opposite.

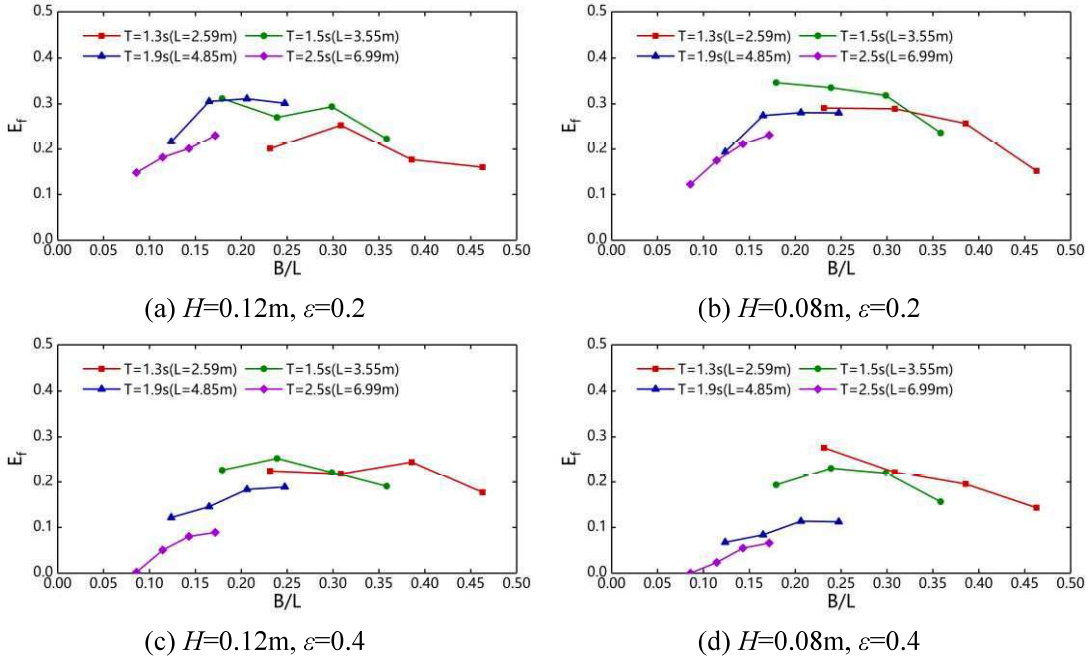

(a) H=0.12m, ε=0.2 (b) H=0.08m, ε=0.2

(c) H=0.12m, ε=0.4 (d) H=0.08m, ε=0.4

Fig. 24 Effect of B/L on wave force reduction coefficient

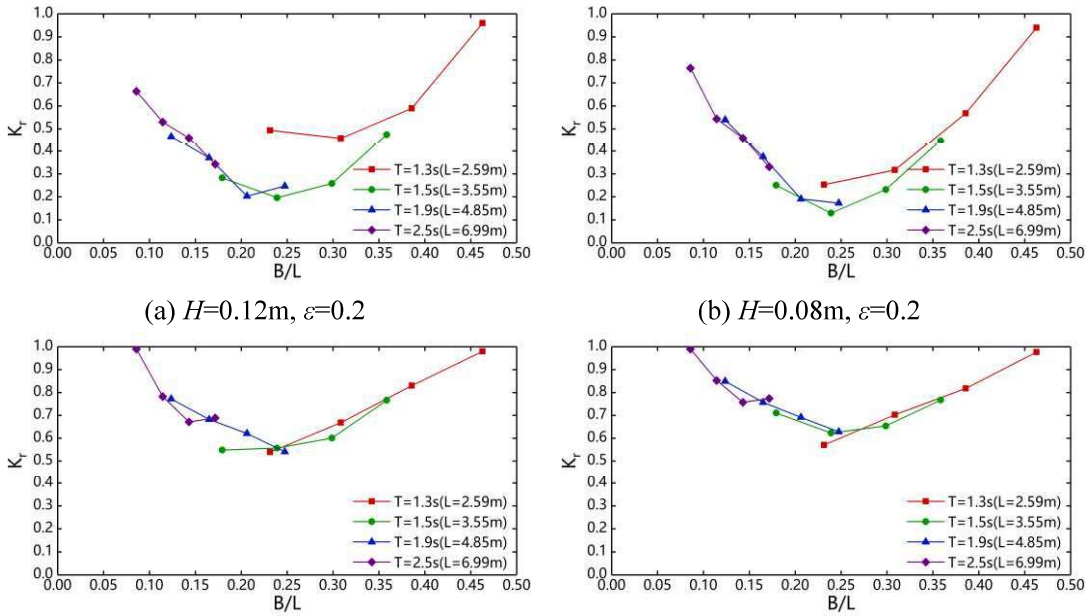

(a) H=0.12m, ε=0.2 (b) H=0.08m, ε=0.2

(c) H=0.12m, ε=0.4 (d) H=0.08m, ε=0.4

Fig. 25 Effect of B/L on the reflection coefficient

Figures 24-25 show the wave force reduction coefficient E_f and reflection coefficient K_r varying against B/L, respectively. It can be seen from the results of

E_f and K_r that some difference occurs when the B/L and other conditions are the same but L is different, which meaning that the wave force reduction effect is different for different wave conditions. On the whole, with B/L increasing from 0 to 0.5, the value of E_f goes up first and then goes down, and the variation of K_r is on the opposite. The largest E_f and smallest K_r appear when B/L ranging from 0.2 to 0.3, where the total wave force is reduced to the smallest.

4.3. Effects of wave height

According to the potential flow theory, the horizontal wave force on a single solid wall increases linearly with the increase of wave heights (Li and Teng, 2015). However, considering the effects of boundary condition of porous barrier for thin porous structures, the relationship between the incident wave height and the wave force on the structures still needed to be studied. In this section, a series of CFD simulations are conducted under different wave heights with the gap width B=0.6m and porosity ε =0.2. The results of present CFD method are compared with a linear potential flow model (Geng et al., 2018).

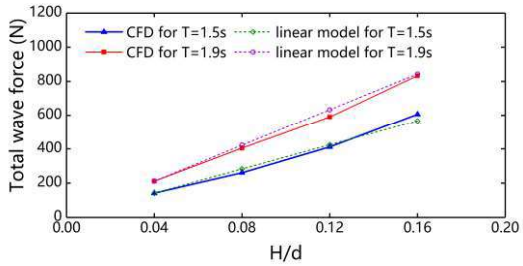

Fig. 26 Wave force varying against H/d by present CFD method and the linear model

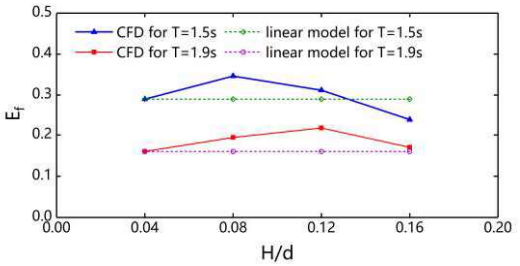

Fig. 27 E_f varying against H/d by present CFD method and the linear model

Figure 26 shows the horizontal wave force amplitude varying against the relative wave heights H/d. It can be seen form Figure 26 that the wave force predicted by the linear model increases linearly with H/d increasing. In contrast, although the wave force predicted by present CFD model also increases with H/d increasing, the relationship between the two is not linear. This will be obvious when comparing the dimensionless coefficient E_f, as shown in Figure 27. The difference above can be explained as follows: according to the Airy wave theory, the motion velocity of water particles in wave is linearly related to wave amplitude, while the wave force on the vertical porous plate is linearly related to pressure drop. This means that the relationship

of velocity and pressure drop determines the relationship of wave force and wave height. Therefore, the linear pressure drop model leads to a linear relationship between the wave height and horizontal wave force on the porous plate and the solid wall, thus the total horizontal wave force is linearly related to the incident wave height. While the present CFD method adopts the quadratic pressure drop condition, and the increase of incident wave amplitude will cause the nonlinear increase of wave force on the porous plate, thus the total horizontal wave force is nonlinear related to the incident wave height. The discussion above illustrated that the quadratic pressure drop condition is essential when studying the wave force on thin porous structures under varying wave heights.

5. Conclusions

For the investigation of the wave load reduction effect of a porous plate on offshore structures, this paper established a CFD numerical model that applied a macroscopic approach for modeling the porous plate. The established CFD model is firstly applied to simulate the interaction between wave and a single vertical porous plate and compared to a microscopic approach and experiment for validation. As a simplified porous structure, a solid wall with a porous plate in front is applied to investigate the wave force reduction effect of the porous plate on the offshore structure. The wave force, wave force reduction coefficient and reflection coefficient were analyzed, with the variation of porosity and relative gap width between the porous plate and solid wall. Several conclusions are obtained as follows:

(1) By comparing with a microscopic CFD approach, it is validated that neglecting the linear and transient terms in pressure loss is reasonable for the CFD numerical model using a macroscopic approach. By comparing with experiments, the established CFD model is validated to be reliable for simulating the interaction between wave and porous plate.

(2) The variation of porosity has effects on wave force reduction. As porosity ε increasing from 0.1 to 0.4, the wave force on the porous plate decreases gradually while the wave force on the solid wall is opposite. The variation of wave force reduction coefficient and reflection coefficient are negatively correlated as expected. The wave force reduction coefficient of whole structure approaches largest at ε=0.2 under most simulated wave conditions except for the wave conditions of H=0.12m, T=1.3s and

H =0.08m, T =1.3s, where E_f reaches the largest value at ε =0.1 and 0.3, respectively.

(3) The gap width between the porous plate and wave length of incident wave influences the phase difference of the wave force on the porous plate and the solid wall, thus affecting the wave force reduction effect. For L=2.69m and 3.55m, as the relative gap width B/L increasing at corresponding ranges, the wave force on porous plate increases gradually, and the wave force on solid wall is opposite; while for L=4.85m and 6.99m, the variation laws above are on the opposite. With B/L increases, the wave force reduction coefficient goes up first and then goes down, and the variation of K_r is on the opposite. The largest E_f and smallest K_r appear when B/L ranging from 0.2 to 0.3, where the total wave force is reduced to the smallest.

(4) The wave height has directly influence on the magnitudes of wave force on the porous structure. The wave force increases nonlinearly with the increase of wave heights, and the quadratic pressure drop condition is essential when studying the wave force on thin porous structures.

Acknowledgments

This work was supported by National Key R&D Program of China [Grant No. 2018YFB1501905], National Natural Science Foundation of China [Grant Nos. 51979030, 51761135011], EPSRC (UK) grant for the project 'Resilient Integrated-Coupled FOW platform design methodology (ResIn)" [Grant No. EP/R007519/1], and Fundamental Research Funds for the Central Universities.

References

Ajiwibowo H., 2011. 2-D physical modeling to measure the effectiveness of perforated skirt breakwater for short-period waves. ITB Journal of Engineering Science, 43, 57-78.

Andersen T. L., Burcharth H. F., Gironella X., 2011. Comparison of new large and small scale overtopping tests for rubble mound breakwaters. Coastal Engineering, 58(4), 351-373.

Bergmann H., Oumeraci H., 1998. Wave pressure distribution on permeable vertical walls. Coastal Engineering, 2042-2055.

Chen B., Wang L., Ning D., Johanning L., 2019. CFD Analysis on wave load mitigation

effect of a perforated wall on offshore structure. Proceedings of the Twenty-ninth International Ocean and Polar Engineering Conference, Honolulu, Hawaii, USA, 3653-3658.

Chen X. Li Y. Sun D., 2002. Regular waves acting on double-layered perforated caissons. Proceedings of the International Offshore and Polar Engineering Conference, 12, 736-743.

Dalrymple R. A., Losada M. A., Martin P. A., 1991. Reflection and transmission from porous structures under oblique wave attack. Journal of Fluid Mechanics, 224, 625-644.

Darcy H., 1956. Les fontaines publiques de la ville de Dijon. Dalmont, Paris.

del Jesus M., Lara J. L., Losada I. J., 2012. Three-dimensional interaction of waves and porous structures. Part I: Numerical model formulation. Coastal Engineering, 64, 57-72.

Fang Z., Xiao L., Kou Y., Li J., 2018. Experimental study of the wave-dissipating performance of a four-layer horizontal porous-plate breakwater. Ocean Engineering, 151, 222-233.

Forcheimer P., 1901. Wasserbewegung durch Boden. Z. Ver. Dtsch. Ing, 45, 1782-1788.

Francis V., Ramakrishnan B., Rudman M., 2020. Experimental investigation on solitary wave interaction with vertical porous barriers. Journal of Offshore Mechanics and Arctic Engineering-transactions of the ASME, 142(4), 041205.

Geng B., Wang R., Ning D., 2018. The wave absorption efficiency of multi-layer vertical perforated thin plates. Journal of Hydrodynamics, 30(5), 898-907.

Goda, Y., Suzuki Y., 1976. Estimation of incident and reflected waves in random wave experiments. Proceedings of the 15th Coastal Engineering Conference, Honolulu, Hi, ASCE, 828-845.

Higuera P., Lara J. L., Losada I. J., 2014. Three-dimensional interaction of waves and porous coastal structures using OpenFOAM®. Part I: Formulation and validation. Coastal Engineering, 83, 243-258.

Hirt C. W. and Nichols B. D., 1981. Volume of fluid (VOF) method for the dynamics of free boundaries. Journal of Computational Physics, 39(1), 201-225.

Huang Z., He F., Zhang W., 2014. A floating box-type breakwater with slotted barriers. Journal of Hydraulic Research. 52(5), 720-727.

Kou Y., Xiao L., Liu J.H., Yang L.J., 2016. Experimental research on the wave-breaking chambers of very large floating offshore base. Journal of Ship Mechanics, 20(07),

833-840.

Koley, S., 2020. Water wave scattering by floating flexible porous plate over variable bathymetry regions. Ocean Engineering, 214, 107686.

Lee J.I., Kim Y.T., and Shin S.,2014. Experimental studies on wave interactions of partially perforated wall under obliquely incident waves. The Scientific World Journal, 954174.

Li Y. and Teng B., 2015. Wave Action on Maritime Structures. China Ocean Press, Beijing.

Liu J., Lin G., Li J., 2012. Short-crested waves interaction with a concentric cylindrical structure with double-layered perforated walls. Ocean Engineering, 40, 76-90.

Liu P., Lin, P., Chang, K., Sakakiyama, T., 1999. Numerical Modeling of Wave Interaction with Porous Structures. Journal of Waterway, Port, Coastal, and Ocean Engineering, ASCE, 125, 322-330.

Liu Y., Li H.J., 2014. Wave scattering by dual submerged horizontal porous plates: Further results. Ocean Engineering, 81, 158-163.

Mackay E., Johanning L., 2020. Comparison of analytical and numerical solutions for wave interaction with a vertical porous barrier. Ocean Engineering, 199, 107032.

Mackay, E., Johanning, L., Qiao, D., Ning, D., 2019. Numerical and experimental modelling of wave loads on thin porous sheets. Proceedings of the 38th International Conference on Ocean, Offshore and Arctic Engineering, OMAE, 2019-95148.

Madsen, P.A., 1983. Wave reflection from a vertical permeable wave absorber. Coastal Engineering, 7, 381–396.

McIver, P., 1998. The blockage coefficient for a rectangular duct containing a barrier with a circular aperture. Applied Ocean Research, 20, 173-178.

Mei, C., Liu, P., Ippen, A., 1974. Quadratic loss and scattering of long waves. Journal of Waterway, Port, Coastal and Ocean Engineering, 100, 217-239.

Mohapatra S. C., Soares C. G., 2020. Hydroelastic response of a flexible submerged porous plate for wave energy absorption. Journal of Marine Science and Engineering, 8(9), 698.

Molines, J., Bayón, A., Gómez-Martín, M. E., Medina, J. R., 2020. Numerical Study of Wave Forces on Crown Walls of Mound Breakwaters with Parapets. Journal of Marine Science and Engineering, 8(4), 276.

Molin B., 2011. Hydrodynamic modeling of perforated structures. Applied Ocean

Research, 33(1), 1-11.

Na'im I., Shahrizal A. Safari M., 2018. A Short Review of Submerged Breakwaters, MATEC Web of Conferences, 203: 01005.

Qiao D., Feng C., Yan J., Liang H., Ning D., Li B., 2020. Numerical simulation and experimental analysis of wave interaction with a porous plate. Ocean Engineering, 218, 108106.

Polubarinova-Kochina, P., 1962. Theory of ground water movement. Princeton University Press, Princeton.

Ren X. and Ma Y., 2015. Numerical simulations for nonlinear waves interaction with multiple perforated quasi-ellipse caissons. Mathematical Problems in Engineering Theory Methods & Applications, 895673.

Smith M. J. A., Peter M. A., Abrahams I. D. and Meylan M. H., 2020. On the Wiener-Hopf solution of water-wave interaction with a submerged elastic or poroelastic plate. Proceedings of the Royal Society A, 476, 20200360.

Sankarbabu K., Sannasiraj S. A., Sundar V., 2008. Hydrodynamic performance of a dual cylindrical caisson breakwater. Coastal Engineering, 55(6), 431-446.

Sollitt C. K. and Cross R. H., 1972. Wave Transmission through Porous Breakwaters. In: Proceedings of 13th Conference on Coastal Engineering, ASCE, 3, 1827-1846.

Teng B., Zhang X., Ning D., 2004. Interaction of oblique waves with infinite number of perforated caissons. Ocean Engineering, 31, 615-632.

Wu Y., Yeh C., Hsiao S., 2014. Three-dimensional numerical simulation on the interaction of solitary waves and porous breakwaters. Coastal Engineering, 85, 12-29.

Yueh C. Y., Chuang S. H., 2009. The reflection of normal incident waves by absorbing-type breakwaters. China Ocean Engineering, 23, 729-740.

Zheng S. M., Meylan M. H., Fan L., Greaves D., Iglesias G., 2020a. Wave scattering by a floating porous elastic plate of arbitrary shape: A semi-analytical study. Journal of Fluids and Structures, 92, UNSP, 102827.

Zheng S. M., Meylan M. H., Greaves D., Iglesias G., 2020b. Water-wave interaction with submerged porous elastic disks. Physics of Fluids, 32(4), 047106.

Zheng S. M., Meylan M. H., Zhu G., Greaves D., Iglesias G., 2020c. Hydroelastic interaction between water waves and an array of circular floating porous elastic plates. Journal of Fluid Mechanics, 900.